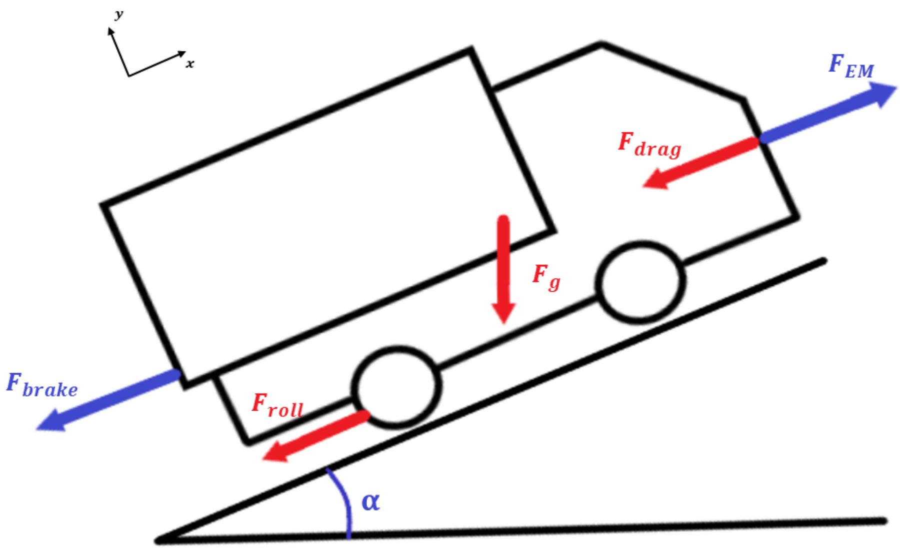

Safety-Aware Predictive Propulsion Control for Heavy-Duty Electric Vehicles

Optimizing vehicle velocity for energy efficiency while maintaining safe operating conditions for the brake and motor systems

Master's thesis in Systems, Control and Mechatronics

Erik Börve

DEPARTMENT OF ELECTRICAL ENGINEERING
Chalmers University of Technology
Gothenburg, Sweden 2022
www.chalmers.se

Master's thesis 2022

Safety-Aware Predictive Propulsion Control for Heavy-Duty Electric Vehicles

Optimizing vehicle velocity for energy efficiency while maintaining safe operating conditions for the brake, motor and battery systems

Erik Börve

Department of Electrical Engineering
Division of Systems and Control
Chalmers University of Technology
Gothenburg, Sweden 2022

Safety-Aware Predictive Propulsion Control for Heavy-Duty Electric Vehicles
Optimizing vehicle velocity for energy efficiency while maintaining safe operating conditions for the brake, motor and battery systems
ERIK BÖRVE

Supervisor: Johannes Brandt, Simulation Engineer, Volvo Group Trucks Technology
Examiner: Nikolce Murgovski, Associate Professor, Department of Electrical Engineering

Master's Thesis 2022
Department of Electrical Engineering
Division of Systems and Control
Chalmers University of Technology
SE-412 96 Gothenburg
Telephone +46 31 772 1000

Cover: Different forces acting on a truck traveling uphill, by Erik Börve.

Typeset in LaTeX
Printed by Chalmers Reproservice
Gothenburg, Sweden 2022

Safety-Aware Predictive Propulsion Control for Heavy-Duty Electric Vehicles
Optimizing vehicle velocity for energy efficiency while maintaining safe operating conditions for the brake, motor and battery systems
ERIK BÖRVE
Department of Electrical Engineering
Chalmers University of Technology

Abstract

The purpose of this thesis is to try and ensure that the brake and motor drive systems are being operated under safe conditions, while maximizing the vehicles energy efficiency. This is accomplished by using model predictive control to optimize the speed, brake temperature and motor temperatures over a horizon of 5 km. The speed is selected to be as close to the reference speed limit as possible while ensuring that the brake and motor power demands does not cause the respective temperatures to exceed safety critical limits. Efforts have also been dedicated to try and ensure that the available motor power does not decrease aggressively. To achieve a more computationally efficient and practically feasible solution the obtained optimal control policy has been approximated using a heuristic algorithm. This heuristic algorithm aims to ensure the safety criteria in terms of brake temperature, electric motor temperatures and motor power decrease.

This thesis produces three different controllers. One optimal controller with the sole objective of limiting brake temperature ("Safe-PEM"), one optimal controller with the objective of liming brake and motor temperature with a less aggressive power decrease ("Safe-PEM with EM") and lastly a heuristic algorithm that accomplishes all of the above ("Heur-PEM"). The results show that it is possible to limit the brake temperature in all three controllers. It is also possible to limit the electric motor temperatures for the Safe-PEM with EM and the Heur-PEM controllers. With the Heur-PEM controller it also becomes possible to ensure a substantially less aggressive engine power decrease strategy, however with sub-optimal performance in terms of energy efficiency.

Keywords: Model Predictive Control, Electric Vehicles, Eco-driving, Brake System, Motor System

Acknowledgements

First and foremost I would like to thank my examiner Nikolce Murgovski and my supervisor Johannes Brandt for the very many interesting discussion (that occurred almost every day for portions of the thesis project) and for tons of guidance in general during my thesis, it would likely have been much more difficult to complete the thesis without your continued support. I would also like to thank Mohammad Abdollahpouri, Rafael Smijtink Klüppel, Rahul Nath and Olof Lindegärde for many interesting discussions regarding the control design as well as guidance with the physical modelling. I would also like to thank Erik Ströby for helping out with all the administrative work and for giving me the opportunity for me do to my thesis at Volvo. Lastly I would also like to thank the whole I-See and Simulation teams at Volvos Camp-X for providing me with a great working environment and not to mention, being very nice people in general!

Erik Börve, Gothenburg, Aug 2022

List of Acronyms

Below is the list of acronyms that have been used throughout this thesis listed in alphabetical order:

AC	Alternating Current
BEV	Battery Electric Vehicle
BMU	Battery Management Unit
BP	Battery Pack
DC	Direct Current
DP	Dynamic Programming
EM	Electric Motor
FCHEV	Fuel Cell Hybrid Electric Vehicle
GCW	Gross Combined Weight
ICEV	Internal Combustion Engine Vehicle
IPM	Interior point method
Li-Ion	Lithium Ion Battery
LHS	Left-Hand Side
LQP	Linear Quadratic Program
MPC	Model Predictive Control
NLOPC	Non Linear Optimal Control Problem
PMSM	Persistent Magnet Synchronous Motors
QP	Quadratic Programming
RHS	Right-Hand Side
RK4	Fourth-Order Runge Kutta method
SOC	State-Of-Charge
SOH	State-Of-Health
SOP	State-Of-Power

Nomenclature

Below is the nomenclature of sets, parameters, and variables that have been used throughout this thesis. The used mathematical notations can be summarized as,

- Vectors and vector functions in bold $\mathbf{b}$
- Matrices in bold capital letters $\mathbf{A}$ and matrix entries in lowercase letters, indexed by there position a_{ij}
- Sets in "blackboard bold" capital letters $\mathbb{X}$
- Optimized variables are noted with an asterisk $\mathbf{x}^*$

Parameters

Here follows a list of parameters used throughout the thesis, in order of occurrence.

γ_i	Gear of the electric motor i
m_v	Vehicle mass
C_d	Vehicle drag coefficient
A_p	Projected vehicle area subject to drag
ρ	Air density
g	Gravity constant
r_{whl}	Wheel radius
A_c	Brake chamber diaphragm area
q_c	Brake system lever ratio
μ_{brake}	friction coefficient between brake disc and rotor
η_{brake}	Efficiency parameter for potential brake system mechanical and slip losses
r_{brake}	Brake disc radius
n_{whl}	Number of wheels on a vehicle
n_{whl}^{tru}	Number of wheels on the truck
n_{whl}^{tra}	Number of wheels on the trailer
μ_{chg}	Battery charging efficiency
t_0	Initial time in prediction horizon

t_f	Final time in prediction horizon
Δt	Sampling time of real world system (time interval)
$\Delta\tau$	Sampling time over horizon (time interval)
Δs	Position discretization step (distance interval)
$\mathbf{Q}$	Cost matrix associated with the state and slack variables
$\mathbf{R}$	Cost matrix associated with the control signals
$\mathbf{P}(s_0)$	Matrix of parameters based on initial position of the horizon.
E_{min}	Constraint on minimum allowed vehicle kinetic energy
A_d	Projected brake disc area subject to convection
m_{disc}	Mass of a single brake disc
$\boldsymbol{\xi}$	Parameters fitted to specific heat capacity function
$\boldsymbol{\sigma}$	Parameters fitted to EM heat loss function
m_{EM}	Mass of a single EM
A_{EM}	Projected EM area subject to convection
h_{EM}	Constant heat transfer coefficient
$C_{p,EM}$	Constant specific heat capacity

Variables

Here follows a list of variables used throughout the thesis, in order of occurrence.

t	Time of the real world system
τ	Time over the prediction horizon
s	Distance over the prediction horizon
k	Discrete steps over the prediction horizon
$\mathbf{x}(t)$	State vector
$\mathbf{u}(t)$	Control signal vector
$\boldsymbol{\delta}(t)$	Slack variable vector
$\boldsymbol{\lambda}$	Lagrange variables associated with equality constraints
$\boldsymbol{\mu}$	Lagrange variables associated with inequality constraints
$\mathbf{s}$	Arbitrary slack variables

Functions

Here follows a list of functions used throughout the thesis, in order of occurrence.

$R(\gamma_i)$	Gear box ratio
$F_{drag}(t)$	Drag force action on the vehicle
$F_{roll}(t)$	Rolling resistance force action on the vehicle
$F_{brake}(t)$	The effective brake force acting on the vehicle at the wheels and
$F_{EM,whl}(t)$	The effective EM force acting on the vehicle at the wheels and
$F_g(t)$	The complete gravitational force action on the vehicle
$F_{g,plane}(t)$	The composante gravitational force action on the vehicle parallel to the road
$\alpha(t)$	The road inclination
$v(t)$	Vehicle velocity
$\omega(t)$	Angular velocity
$I_{bat}(t)$	Current supplied to the motor from the battery
$V_{bat}(t)$	Current operation voltage of the battery
$\omega_{EMi}(t)$	Angular velocity of electric motor i
$\mathcal{T}_{EMi}(t)$	Output torque of electric motor i
P_{bat}	Battery power output
$P_{aux}(t)$	Auxiliary power usage
$P_{EM}^{el}(t)$	Electrical power input to a motor
$P_{EM}^{mech}(t)$	Mechanical power output for a motor
$\eta_{EM}^{trac}(t)$	Traction power efficiency
$\eta_{EM}^{gen}(t)$	Power generation efficiency
$P_c(t)$	Brake chamber pressure
$\mathcal{T}_{brake}(t)$	Generated brake torque at the wheels and
$Q(t)$	Battery capacity
$I_{bat}^{dChg}(t)$	Battery discharge current
$I_{bat}^{Chg}(t)$	Battery charge current
$SOC(t)$	Battery state-of-charge
$\mathcal{L}(\mathbf{x}, \boldsymbol{\lambda}, \boldsymbol{\mu})$	Lagrange function
$f_c(t)$	ICE fuel consumption
$D_{log}(k)$	Pre-filter decision log
$V_{log}(k)$	Pre-filter velocity choice
$E_k(k)$	Vehicle kinetic energy
T_{brake}	Brake temperature
$E_{ref}(k)$	Reference kinetic energy based on speed limit
$T_{EMi}(k)$	EM temperature of motor i

$F_{EM}^{max}(\mathbf{x}(k), \mathbf{P}(s_0))$	Maximum EM force constraint based on EM dimensioning
$F_{bat}^{max}(\mathbf{x}(k), \mathbf{P}(s_0))$	Maximum EM force based on batter capacity
$F_{bat}^{min}(\mathbf{x}(k), \mathbf{P}(s_0))$	Minimum EM force based on battery capacity
$F_{EM,c}^{max}(\mathbf{x}(k), \mathbf{P}(s_0))$	Comfort constraint EM force
$F_{brake,c}^{max}(\mathbf{x}(k), \mathbf{P}(s_0))$	Comfort constraint on brake force
$\Delta_F(x_3(k), x_4(k))$	EM temperature dependant constraint on the change in force.
$h_{brake}(t)$	Temperature dependant heat transfer coefficient for the brake disc convection
$C_{p,brake}(t)$	Temperature dependant specific heat transfer coefficient for the brake discs
$P_{EM,loss}(t)$	Angular rate and torque dependant EM heat losses
$\boldsymbol{\beta}(s_0)$	Adaptive parameters fitted in EM temperature model using EKF

Sets

Here follows a list of sets used throughout the thesis, in order of occurrence.

$\mathbb{H}_\infty$	Infinite continuous horizon
$\mathbb{H}$	Finite continuous horizon
$\mathbb{X}$	Set constraint for states $\mathbf{x}$
$\mathbb{U}$	Set constraint for control signal $\mathbf{u}$
$\mathbb{V}$	Discretized set of available velocities
$\mathbb{G}$	Discretized set of available gears

Contents

1

Introduction

1.1 Motivation

As a result of the Paris Agreement established in 2015, the European Union has made large efforts towards decreasing the greenhouse gas emission that stem from overland transport via heavy-duty vehicles. A portion of these efforts has been summarized in the EU-wide emissions standards introduced in 2019, together with quantitative climate goals for 2050 [1]. As the demand for road transport is continuously increasing, these goals are becoming progressively more difficult to reach. At the current rate overall greenhouse emission levels are predicted to decrease by 10% as of 2030, which already is 6% less than what the EU suggests is necessary to fulfill the demands imposed by the Paris Agreement [2]. Further, individual countries like the UK have committed to reduces their greenhouse gas emissions in the transport sector by 80% by 2050 [3]. Clearly there is a need for a rapid improvement if either of these goals are to be meet.

A common proposed approach towards meeting these goals is to further accelerate the transition to fuel cell hybrid electric vehicles (FCHEV) and fully battery electric vehicle (BEV) systems. However, for these systems to be able to compete with conventional internal combustion engine vehicles (ICEV) there are still large challenges to overcome, in terms of e.g., improving range and component life length. One approach to increasing the former is to optimize the efficiency of the transformation from the chemical potential energy in the battery and or fuel cell to the potential and kinetic energy that is required for propulsion. This is also known as the "*tank-to-meter*"-efficiency and depends on a plethora of factors such as, friction and heat losses in the power train. In recent years *Eco-driving* has been a widely considered approach for improving energy efficiency. With this method the idea is to utilize information about upcoming road inclination and traffic to set an appropriate vehicle velocity such that the potential and kinetic energy can be used efficiently. The term *Predictive Propulsion Control* stems from the approach of utilizing information about for example, the future inclination to predict the performance of components in the power train to advance the vehicle in a more energy efficient fashion. This approach has been rigorously studied and has on occasions shown to potentially decrease the energy usage by $\sim 10\%$ in hilly terrain [4, 5, 6].

While much research has been dedicated to improving the energy and computational efficiency, less has been done to investigate how the resulting velocity profile impacts different components in the power train. When considering heavy-duty vehicles in combination with hilly driving cycles, the suggested energy efficient velocity profile might cause large strain on different components, resulting in a practically infeasible and perhaps even dangerous solution. The main purpose of this thesis is to expand on previous work by additionally ensuring safe operations of the braking system. This specifically involves ensuring that the temperature of the brake discs is kept below certain temperatures. This since the usable braking power decreases at extreme temperatures, causing dangerous driving conditions [7].

Additionally, the motor system will also be investigated in a similar fashion. For both these systems, a manual derate in performance occurs during hazardous operating conditions to avoid a sharp decrease in life length and potentially dangerous system failures. In the current case this is accomplished by sharply decreasing the power output of the motor, also referred to as "derating" the motor. In turn this results in a drastic change in the drive-ability of the vehicle which potential could introduce safety issues in certain situations. The purpose of this investigation is to maximize the power output of the motor to meet the demand required to maintain the reference speed limit, while avoiding high internal temperatures and sharp derates in performance.

1.2 Limitations

Since the most safety critical conditions occur for heavy duty vehicles and predominantly hilly cycles, these where both chosen as the main area of interest. In this context heavy duty vehicles are defined as vehicles with a gross combined weight (GCW) of above 46 metric tons. To investigate the impact of different loads, this thesis considers two GCW cases of 46 and 64 tons. Similarly, to investigate varying elevation, three different cycles where investigated. Worth noting, is that the speed limit was set to 80 kmh for the entire duration of all cycles. This to allow for a fairer comparison of the different cases.

To limit the scope of the study, only BEVs were investigated, and the same power train architecture was used in all scenarios. The vehicle investigated in this thesis is a fully electric truck with two separate electric motors (EM) and six battery packs (BP). Similarly, the same vehicle configuration was also used in all scenarios. The configuration includes one main unit which houses e.g., the power train and cabin, together with a second trailer unit which houses the transported cargo. The truck was selected to have six wheels in total, of which two where driven and the trailer was selected to have six wheels in total, of which none where driven. All wheels on the truck and trailer had a separate brake system and the operation of said systems differed between the truck and trailer. Since the systems where identical otherwise, the truck and trailer brakes were assumed as two separate lumped systems. Notably, the activation requirement for the truck brakes were assumed lower than that of the trailer brakes. As suggested by empirical data, this meant that the truck brake temperatures would exceed that off the trailer in all the investigated scenarios. Hence, only the truck brake temperature was considered in the predictive controllers to reduce the computational load. The change in EM and brake temperature where both modelled using first degree approximations, also to reduce computational complexity.

Since the used simulation tool only considers longitudinal dynamics, no lateral dynamics were considered in modeling. In theory this means that the road is considered as perfectly straight and that there are no resulting forces acting outside the plane spanned by the truck's direction of motion and the normal vector of the ground surface. The simulation tool does neither utilize any traffic data and hence neglects any interaction with other vehicles. Notably, since the vehicle configuration includes a trailer, there will likely be significant stability challenges that in this case are neglected. In a practical application this point would be well worth considering. The listed challenges are however considered outside the scope of this thesis.

1.3 Main Research Questions

The research questions that are covered in this thesis can be summarized as follows,

- Is it possible to ensure that the temperature of the brake discs is kept below a certain level via optimal control while optimizing the vehicles energy efficiency?
- Is it possible to ensure that the electric motor temperatures are kept below a certain level via optimal control while optimizing the vehicles energy efficiency?
- Is it possible to limit the motor temperature by using a less aggressive power derate-strategy via optimal control while optimizing the vehicles energy efficiency?
- If the above questions are feasible, is it possible to archive a safe operation of the brakes and motor system using a more computationally efficient heuristic control strategy?

2
Theoretical Background

This section aims to introduce the necessary theory required to accurately follow the execution of the remainder of the thesis. Note that some content has been obtained in discussion with representatives at Volvo and hence some details have been omitted for confidentiality reasons.

2.1 Vehicle Modelling & Theory

2.1.1 Vehicle Architecture

As the name suggests, battery electric vehicles (BEVs) are defined as vehicles that are fully powered by electrical energy, which mainly is stored in battery packs. A schematic illustration of the key components of the studied power train is displayed below in Figure 2.1.

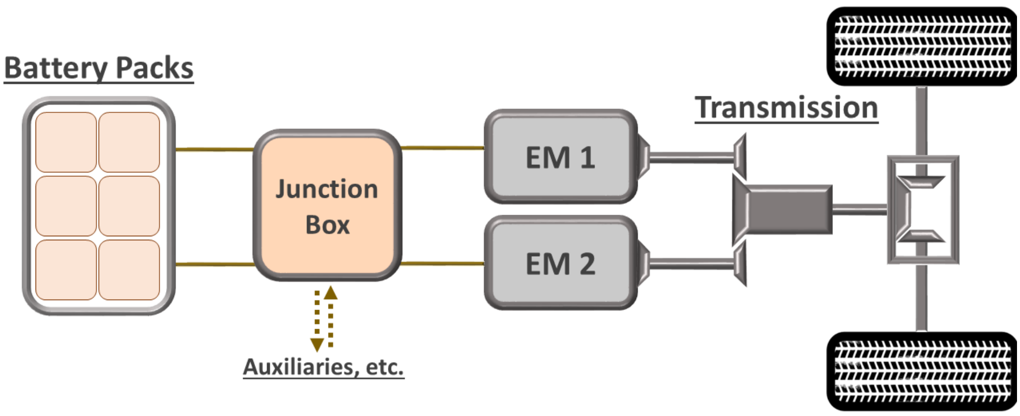

Figure 2.1: A schematic illustration of the power train in the investigated BEV.

The architecture consists of 6 separate battery packs that transports energy to and from a junction box. This junction box is then responsible for distributing the power throughout all components of the vehicle. This includes everything from auxiliaries and charging, to the electric motors. The studied vehicle utilizes two separate motors, noted below as EM1 and EM2, that supply torque to and from the transmission. The transmission is then further connected to the drive axis which supplies the torque to the wheels and causes propulsion. Notably, the two motors both contribute to driving the same axle but are in theory otherwise decoupled from each other. This means that it becomes possible to operate the respective motor independently from the other to control e.g., their respective temperatures. In practice this is determined by the gearbox which can be considered as a subsystem of the transmission. Notably, the gearbox introduces a gear ratio $R(\gamma)$ depending on the current gear γ. As also introduced earlier, the vehicle configuration includes a main truck and a trailer. Both the truck and trailer have 6 separate wheels respectively, of which all are fitted with a mechanical brake system and the two rear wheels on the truck are driven. The wheelbase structure in relation to the power train is displayed in Figure 2.2.

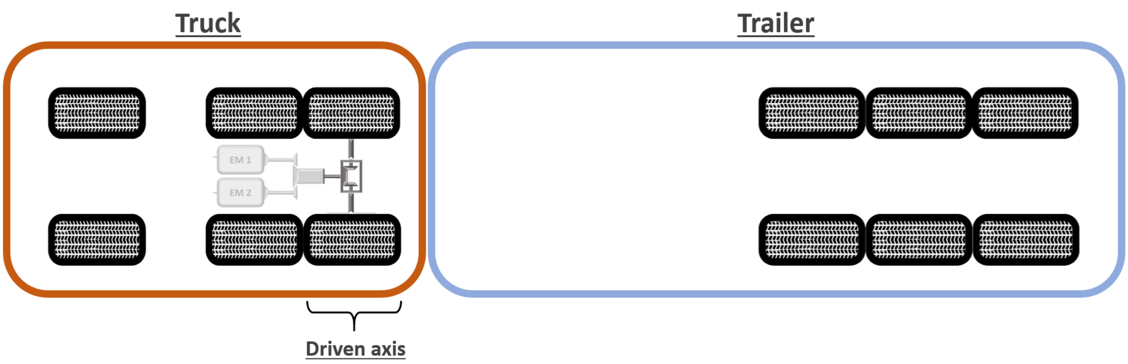

Figure 2.2: wheelbase configuration of the investigated vehicle architecture.

2.1.2 Longitudinal Vehicle Dynamics

Since lateral dynamics are neglected, the core concept for modelling the vehicle velocity is naturally to model the dynamics along the axis that is aligned with the road, also knows as the longitudinal dynamics. This approach is well documented in literature and generally follows the system structure illustrated below in Figure 2.3 [8, 9]. The fundamental interpretation of this model is that the propulsion system produces mechanical energy that is momentarily "stored" as kinetic and potential energy. The corresponding retarding forces are then assumed to drain energy from this reservoir. With this simple model the energy losses origin from the aerodynamic friction ($F_{drag}(t)$), the rolling friction losses ($F_{roll}(t)$) and the heat dissipation in the mechanical brakes ($F_{brake}(t)$). Energy is supplied to the system when the force at the wheels, which in turn is generated from the engine ($F_{EM,whl}(t)$), is positive. The energy of the vehicle is also recuperated back into the power train as electrical energy when the force is negative. The gravitational force ($F_g(t)$) introduces an additional retarding or propelling force along the plane depending on the road topography's inclination (α).

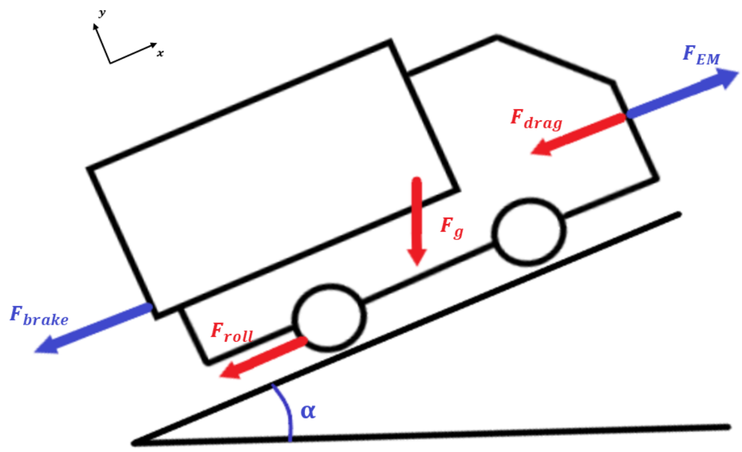

Figure 2.3: Visualization of the considered forces acting on a vehicle traveling along an inclined road.

When constructing a mathematical model of the above system the vehicle is typically considered as a point mass. By placing the x-axis such that it is parallel to the ground and the y-axis such that it is normal the ground surface the force balance can be expressed as,

$$m_v \frac{\partial^2}{\partial t^2} x(t) = F_{EM,whl}(t) + F_{brake}(t) + F_{roll}(t) + F_{g,plane}(t) + F_{drag}(t) \tag{2.1}$$

where the vehicle mass (m_v) is assumed constant by neglecting the impact of inertial mass effects from e.g., the motor and wheels. The drag force is typically considered to be proportional to the square of the vehicle velocity. By considering the aerodynamic friction and the impact of pressure differences it is possible to express the proportionality constant as follows,

$$F_{drag}(t) = -Cv(t)^2 = -\frac{C_d A_p \rho v(t)^2}{2} \tag{2.2}$$

where C_d is the drag coefficient, A_p is the projected area of the vehicle perpendicular to the air flow and ρ is the air density [10].

Further, the rolling resistance can be expressed via the normal force as,

$$F_{roll}(t) = -c_r F_N(t) = -c_r m_v g \cos(\alpha(t)) \tag{2.3}$$

where the gravitational force has been projected on the y-axis based on the inclination. In a similar fashion this also yields the impact of the gravitational force on the x-axis,

$$F_{g,plane}(t) = -m_v g \sin(\alpha(t)) \tag{2.4}$$

2.1.3 Electric Motors

Generally speaking, the field of electric motors can be separated in two main subcategories, alternating current (AC) and direct current (DC) motors. The name of the two motor classes stems from their respective type of input current which also changes the method of the electromechanical energy conversion. In practice this means that the two types are suitable for some applications but can be infeasible in others. For applications within large electric vehicles there exists a high demand on efficiency and torque density to e.g., maximize the range. All though DC motors exists with desirable properties in this regard (e.g., brushless DC motors), the state-of-the art performance for the application within heavy-duty electric trucks is currently obtained using AC motors. AC motors do however come with an increase cost of hardware, e.g., because they require an inverter to transform the DC current that is supplied from the battery. Regardless, AC motors will be the focus of this thesis [11]. The basic working principle of an AC motor revolves around using a stator that creates a rotating magnetic field. A schematic illustration of a basic motor construction is displayed in Figure 2.4a.

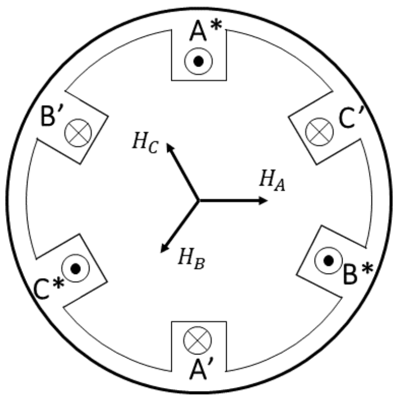

(a) Schematic illustration of a 3-phase alternate current motor with two poles.

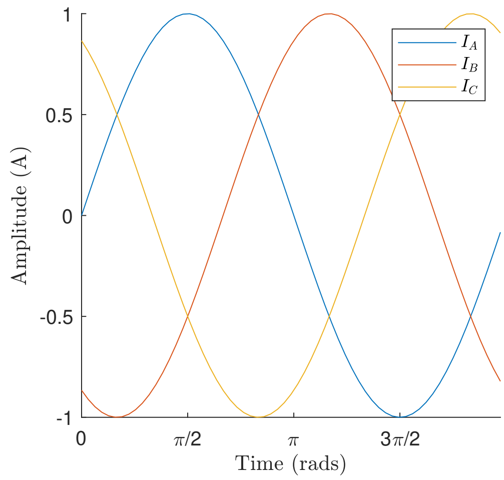

(b) Example of current flow through the respective coils over one period.

Figure 2.4: Working principle of a basic alternating current motor, re-worked from Chapman S.J (2004) [12].

This motor includes 3 separate sets of windings (marked A-C) with 2 respective poles. Alternating Current is supplied to the end of the coils marked ($\bullet'$) which flows back and forth over the motor and leaves at the ends marked ($\bullet^*$). As current flows through the respective coils a magnetic field is generated in accordance with Faradays law. The rotation in the sum of these fields is generated by introducing a phase shift in the current that is supplied to the respective coils. In the below example where three separate coils are used, this phase shift typically corresponds to 120^o. An example of the resulting current with angular velocity $\omega = 1\ \frac{\text{rad}}{\text{s}}$ is displayed in Figure 2.4b. The amplitude and sign of each current is hence directly related to magnitude and direction of the generated magnetic field of the corresponding winding. This is marked in Figure 2.4a as H_{A-C} [12].

When designing the rotor magnet there are typically two different approaches, induction rotors and permanent magnet rotors. The induction motor rotor consists of a “cage” of electrical wires which are connected to an “end ring”. When the stator magnetic field rotates a current will be induced in the cage wiring. This will in turn cause the rotor to rotate in accordance with Lorentz law which produces the torque output from the motor. In essence, the rotor becomes an electromagnet which attempts to align its poles with the rotating magnetic field of the stator. Since the magnetic field in the rotor is induced by the stator, the rotor speed will never reach that of the stator. This introduces a lag between the stator and rotor which is why the induction motors are referred to as “asynchronous”. This slip usually accounts for an approximately 5% decrease in efficiency [13]. The other common approach instead utilizes a rotor that itself generates a permanent magnetic field. Typically, in the AC case this means that permanent magnets are placed in a certain pattern matching the poles on the stator. Since the corresponding poles on the stator and rotor will be attracted to each other the rotor will rotate with the same speed as that of the stator magnetic field. Hence, this class of motors are referred to as permanent magnet synchronous motors (PMSM) [14] Due to the lack of slip between the rotor and stator the PMSM motors are generally more controllable and efficient. This in combination with high torque densities makes them desirable for the application within BEV which also is why they will be studied in this thesis.

Further, with the two-pole-setup, it can be shown that the rotating magnetic field completes one rotation about the stator per period of supplied voltage, i.e., the frequency of the supplied current and the rotating magnetic field is identical. It can also be shown that if the rotation of the magnetic field is reversed, so is the direction of the stator current. Hence, by applying torque to the rotor it becomes possible to revert the rotation of the magnetic field and transfer energy from the vehicle propulsion to the battery. This means that the EM can operate both as an engine and as a generator. This is particularly useful when braking the vehicle and means that it is possible to recuperate some of the kinetic energy that is lost when the vehicle decelerates. The extend to which this is possible is constrained not only by the amount of power that the engine can supply, but also by the amount of energy the battery is able to accept. The amount of energy that the battery is able to accept is further dependant on the current power demand of other auxiliary components on the vehicle.

To ensure that the stator magnetic field is maintained it is crucial to use a robust winding construction. One key factor is to insulate each wire to avoid short circuiting the whole engine, causing an expensive repair. Since the insulation is sensitive to high temperatures it is important to ensure that the winding temperature is not kept above a certain temperature limit for an extended period of time. To quantify this impact, it is common to introduce a state-of-health (SOH) metric which aims to predict the likelihood of future engine failures. To circumvent the overheating issue, the engine windings are cooled using fans or by simply forcing the engine to decrease the amount of used power, which is quantified by a so-called state-of-power (SOP).

This approach is also referred to as “derating” the engine. In both these cases it is not straight forward to determine to what extent it is necessary to cool or derate the engine to ensure that overheating is avoided. This since the winding temperature indirectly is heavily dependant on the upcoming road topography. In practice, using controllers without predictive models, this typically results in an excessive amount of energy spent on cooling or an excessive decrease in the drive-ability of the vehicle.

Modelling

By neglecting losses in wires between components and power converters it becomes possible to obtain a relation for the motor power input using the current ($I_{bat}(t)$) and voltage ($V_{bat}(t)$) that is supplied by the battery together with a prediction of the power usage of the auxiliaries ($P_{aux}(t)$). The power output from the motor is described by the rotors angular velocity $\omega_{EM}(t)$ and torque $\mathcal{T}_{EM}(t)$ as,

$$P_{EM}^{El}(t) = I_{bat}(t)V_{bat}(t) - P_{aux}(t) \tag{2.5a}$$

$$P_{EM}^{Mech}(t) = \omega_{EM}(t)\mathcal{T}_{EM}(t) \tag{2.5b}$$

This naturally leads to a definition of the engine efficiency η_{EM} which can be defined in two ways depending on if the motor is consuming or generating power,

$$\eta_{EM}^{trac}(t) = \frac{P_{EM}^{Mech}(t)}{P_{EM}^{El}(t)} \tag{2.6a}$$

$$\eta_{EM}^{gen}(t) = \frac{P_{EM}^{El}(t)}{P_{EM}^{Mech}(t)} \tag{2.6b}$$

where η_{EM}^{trac} denotes the efficiency when the engine is consuming power and supplying a traction force to the wheels and η_{EM}^{trac} denotes the efficiency when the engine is generating power that is converted to electrical energy and is stored in the battery. Both efficiency metrics are typically estimated based on the angular velocity and torque of the motor. One example of such an efficiency map is displayed below in Figure 2.5.

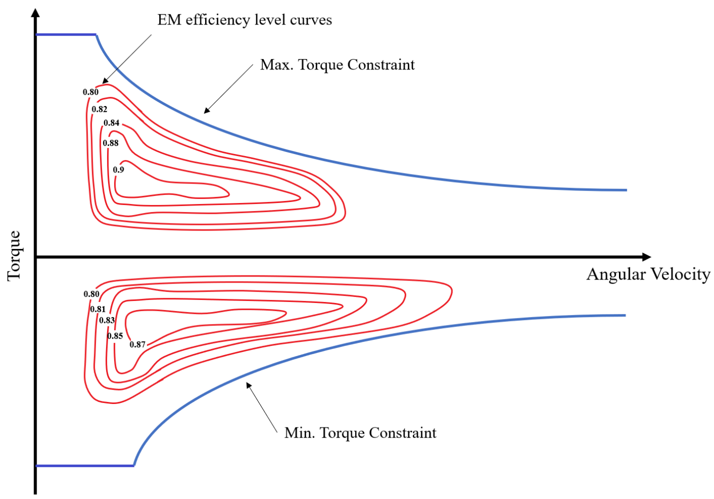

Figure 2.5: Efficiency map of an PMSM electric motor, based on the rotational speed and torque of the motor, adapted from[15].

The torque output from the engine is then supplied to the drive axis via the transmission. The input and output torque from the transmission system is related to each other via the gear ratio $R(\gamma_i)$ which is a function of the gear (γ_i) of each respective motor $(i = 1, 2)$. The total torque supplied to the drive axis will correspond to the sum of the contribution from each engine, multiplied by the torque ratio at the drive axis (R_{fgr}). The EM torque can finally be connected to the force at the wheels via their radius (r_{whl}) as,

$$F_{EM,whl}(t) = \frac{R_{fgr}}{r_{whl}}\Big(\eta_{EM1}(t)R(\gamma_1)\mathcal{T}_{EM,1}(t) + \eta_{EM2}(t)R(\gamma_2)\mathcal{T}_{EM,2}\Big) \tag{2.7}$$

which then can be related to the longitudinal vehicle dynamics as described by Equation (2.1). Notably the angular rate of the respective motor can also be predicted based on the current vehicle velocity $v(t)$ as,

$$\omega_{EM,i} = \frac{R(\gamma)}{r_{whl}}v(t) \tag{2.8}$$

where $v(t)$ can be obtained from solving the force balance Equation (2.1).

2.1.4 Mechanical Brake Systems

Developing a safe braking system for heavy-duty vehicles is particularly challenging problem due to the increased demand on available brake power. In modern applications air disc brakes are preferred over the traditional drum brakes. This is partially since the disc brakes are more exposed to the surrounding air which increases cooling via natural convection. A schematic illustration of an air disc brake configuration is displayed in Figure 2.6. The fundamental idea of this system is to transfer air pressure into friction force. To quickly summarize the principle of operation, when the brakes are activated air flows into the service brake chamber increasing the pressure. As the pressure increases the diaphragm will cause the push rod to supply a force to the socket on the lever. The lever will then pivot around a bearing causing the bridge to move the inner brake disc. This eventually causes both the inner and outer disc to press against the brake rotors which in turn pushes against the wheel, slowing down its rotation via friction [16].

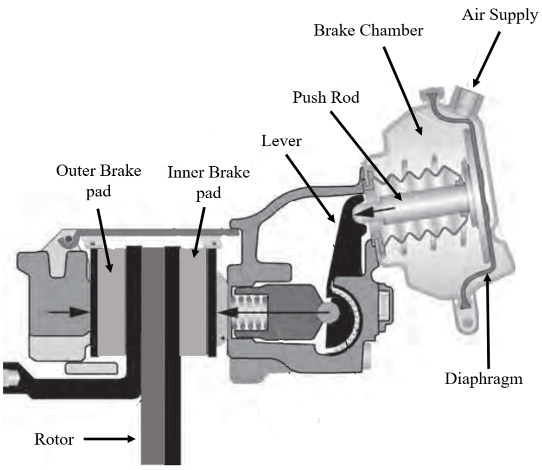

Figure 2.6: Schematic illustration of the key components of an air disk brake system, re-worked from [16].

The purpose of the disc brakes is to transfer the kinetic energy of the vehicle into heat via friction. With a high power demand, the brake discs will absorb a lot of heat causing a sharp increase in temperature. When the discs reach a high enough temperature the available brake power will start to fade. This is partially due to a decrease in the friction coefficient between the discs and the rotor as the brake disc material is less resistant to deformation at high temperatures. Hence, at high enough temperatures, the brake system will experience significant drops in performance which could cause dangerous driving scenarios [17].

Modelling

When estimating the produced brake torque, it is common to assume that the torque is proportional to the pressure in the brake chamber [18]. By using a "quarter-car braking model", i.e. considering only a single wheel and brake system it becomes possible to express the produced brake torque as,

$$\mathcal{T}_{brake}(t) = C_{brake}P_c(t) = 2A_c q_c \mu_{brake} r_{brake} \eta_{brake} P_c(t) \tag{2.9}$$

where A_c is the area of the brake chamber diaphragm, r_{brake} is the radius of the brake discs, q_c is the lever ratio and μ_{brake} is the friction coefficient between the brake disc and the rotor. Additionally, η_{brake} corresponds to an efficiency parameter that is calculated by lumping potential mechanical and slip losses. By further lumping together all individual brake systems on the truck it becomes possible to find a simple relation between the different brake torques and the effective force that can be used in the longitudinal dynamic model,

$$F_{brake}(t) = -n_{whl}\frac{\mathcal{T}_{brake}(t)}{r_{whl}} \tag{2.10}$$

where r_{whl} corresponds to the wheel radius and n_{whl} corresponds to the number of wheels with an active mechanical brake system.

In practice this model is extended by introducing an activation pressure (P_0). The brake torque will hence only be non-zero if the chamber pressure exceeds P_0 which motivates a new formulation of Equation (2.9) as,

$$\mathcal{T}_{brake}(t) = min\Big\{0, C_{brake}\Delta P_c(t)\Big\} \tag{2.11}$$

Also note that the brake chamber pressure has been replaced with deviation from the activation pressure $\Delta P_c(t) = P_c(t) - P_0$. Finally, since the considered vehicle configuration includes a trailer there will exist two separate brake system configurations. The main difference being that the truck brake activation pressure typically is lower than that of the trailer brakes [19]. By lumping the individual brake systems on the truck and trailer separately the total braking force can be expressed as follows,

$$F_{brake}(t) = \frac{1}{r_{whl}}\Big[n_{whl}^{tru} min\{0, C_{brake}^{tru}(P_c(t) - P_0^{tru})\} + n_{whl}^{tra} min\{0, C_{brake}^{tra}(P_c(t) - P_0^{tra})\}\Big] \tag{2.12}$$

which then can be related to the longitudinal vehicle dynamics as described by Equation (2.1) [20].

2.1.5 Batteries

The purpose of batteries for applications within vehicles is to store chemical energy that can be transformed into electrical energy. It should also be possible to reverse this transformation to allow for charging via e.g., regenerative braking and conventional methods. In terms of key performance metrics, the capacity describes the sum of the current that can be delivered over a certain time interval. Typically, the extant capacity is used together with the nominal to describe the state-of-charge (SOC) which hence represents an estimate of how much more energy is available in the battery. To maximize the range of the vehicle it is important to utilize batteries with a high capacity relative to its weight, which is referred to as specific energy.

Similarly, to increase the drive-ability it is also desirable to use batteries with a high power output per weight, referred to as specific power [21].

The most extensively used battery type that achieves state-of-the-art performance in terms of these metrics is the Lithium-ion battery (Li-Ion). The electrochemical galvanic cell of the Li-Ion is displayed below in Figure 2.7. The Figure illustrates the battery operating in discharge with a graphite anode and lithium-doped cobalt oxide ($LiCoO_2$) cathode. During discharge the lithium ions spontaneously separate from the graphite lattice and travel through the ion-conducting electrolyte in the direction of the electric potential field. The ions eventually travel thought the ion-conducting separator and react with the cathode material and excess electrons. Since neither the electrolyte nor separator conducts electrons, the electrons will mainly travel to cathode via the current collectors connected at each end of the cell. This flow of electrons forms the current that can be used to drive the electrical load. Naturally this current will be of the DC variety. If this flow of electrons is reverted by instead supplying electrical energy at the load it becomes possible to reverse this reaction and convert the electrical energy back to chemical [22].

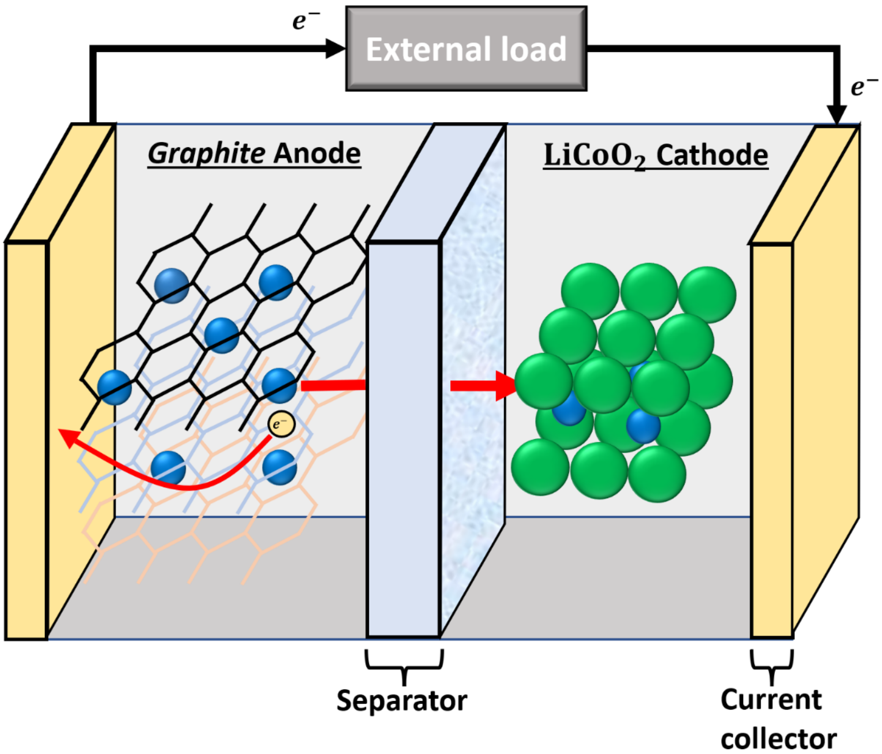

Figure 2.7: The electrochemical process Li-Ion battery, re-worked from [22]. The blue and green spheres represent lithium and cobalt respectively.

The above chemical process can be summarized in the following redox reactions. The negative electrode half-cell reaction at the anode follows,

$$\mathrm{LiC_6} \leftrightharpoons \mathrm{C_6} + \mathrm{Li^+} + \mathrm{e^-}$$

and the corresponding positive electrode half cell reaction at the cathod follows,

$$CoO_2 + Li^+ + e^- \leftrightharpoons LiCoO_2$$

Combining the two half-cells yields the overall redox reaction as,

$$CoO_2 + LiC_6 \leftrightharpoons LiCoO_2 + LiC_6$$

Note here the bi-directional arrows that indicate that the reaction is reversible which allows for both charging and discharging of the battery [23].

In heavy duty vehicle applications, the demand on the electric motor power will be large, especially in up- and down hills. This naturally translates to a large demand on the battery power, not only in terms off discharging the battery to match traction power request but also in terms of charging to match the regenerative brake power demand. Since the electrochemical process mentioned above is relatively involved and can be influenced by many different factors, it becomes quite challenging to make an accurate prediction of the maximum available power [24]. To estimate the long term change in charge and discharge power-ability it is possible to express these as functions of the SOC and battery temperature. Figure 2.8 displays this dependence for both the discharge and charge operations. Note that the battery is able to discharge quickly at high SOC and temperature as well as charge quickly at low SOC and high temperatures.

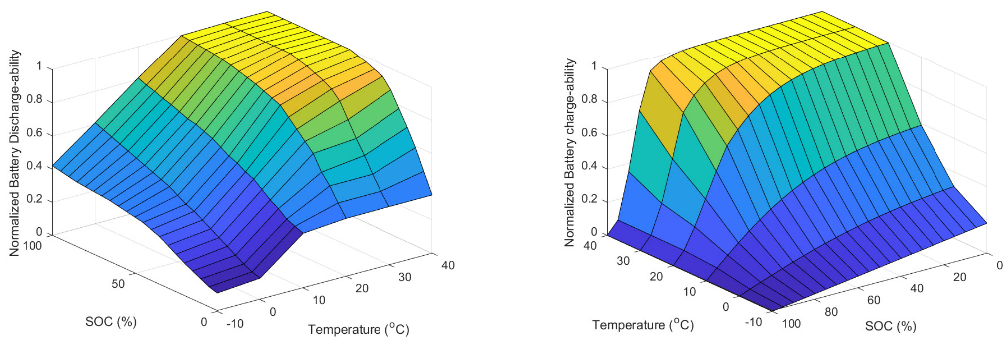

(a) Normalized discharge-ability for a battery depending on SOC and temperature.

(b) Normalized discharge-ability for a battery depending on SOC and temperature.

Figure 2.8: Normalized Charge- and discharge-ability for a battery, adapted from [25].

Modelling

During discharge the change in battery capacity ($\dot{Q}(t)$) is directly proportional to the instantaneous current ($I_{bat}^{dChg}(t)$ or $I_{bat}^{Chg}(t)$) as seen below. This also naturally leads to a definition of the capacity via simple integration.

$$\dot{Q}(t) = -I_{bat}^{dChg}(t) \tag{2.13}$$

$$Q(t) = \int_{t_0}^{t_f} -I_{bat}^{dChg}(t), \quad Q(0) = Q_0 \tag{2.14}$$

where Q_0 represents the nominal capacity. A similar relation is naturally used for the charging operation, however with the introduction of an efficiency parameter (μ_{Chg}) that corresponds to energy losses due to some undesirable irreversible reactions that can occur in the battery. This simply led to the corresponding estimation of the change in capacity during charging as,

$$\dot{Q}(t) = \mu_{Chg} I_{bat}^{Chg}(t) \tag{2.15}$$

This can then be used to estimate the state-of-charge as,

$$SOC(t) = \frac{Q(t)}{Q_0} \tag{2.16}$$

The instantaneous power output can then simply be estimated by,

$$P_{bat}(t) = I_{bat}(t) V_{bat}(t) \tag{2.17}$$

which then can be used to constraint the motor power usage as seen in Equation (2.5a) [15].

Predicting the maximum available power, or peak-power-ability is a problem that still is under investigation in research and currently requires involved models based on e.g., SOC and the battery temperature [26]. For this problem, these metrics would have to be introduced by multiple additional states in the predictive controller. Since the corresponding update equation of said state likely would be non linear this would have resulted in an increasingly difficult optimization problem. Consequently, predicting the power-ability over the horizon has been neglected in this thesis. Instead, the peak-power-ability was obtained from the battery-management-unit (BMU) and assumed constant over the $5km$ long prediction horizon.

2.2 Non Linear Optimal Control

In the broadest sense optimal control concerns methods that determine the control actions $\mathbf{u}(t)$ and state trajectories $\mathbf{x}(t)$ by minimizing a certain objective function $V(t)$. The approach used to solve this optimization problem is in turn highly dependant on different system characteristic. For a simple optimization problem with linear equality constraints and a quadratic objective function (LQP), it becomes possible to obtain an explicit solution for an optimal control law $\mathbf{u}^*(t)$ for all future time $t \in \mathbb{H}_\infty = [t_0, \infty)$. However, for complex real-world applications this is seldom the case. If the system states and control signals are constrained to some sets $\mathbf{x}(t) \in \mathbb{X},\ \mathbf{u}(t) \in \mathbb{U}\ \forall t \in \mathbb{H}_\infty$, for example due to physical limitations on actuators, it is not possible to guarantee that the previous optimal solution can be obtained explicitly. A popular approach to solving this issue is to use constrained receding horizon control, commonly refereed to as Model Predictive Control (MPC). Due to the lack of an explicit solution, it is no longer possible to solve this optimization problem for all future time $\mathbb{H}_\infty$. Instead the optimization problem is formulated for a certain amount of time into the future $\mathbb{H} = [t_0, t_f],\ t_0 < t_f$. This also means that the problem must be solved repeatedly as t increases, meaning that the problem considers $t_0 = t$ and solves the optimization problem over the time horizon $\mathbb{H}$ [27]. Given that the objective function is quadratic, the state dynamics are linear and the sets $\mathbb{X}$, $\mathbb{U}$ have linear boundaries, the resulting problem will be convex, assuming that it also is regular. Via the definition of the objective function and constraints the problem can then be solved efficiently by so-called quadratic programming (QP).

However, as will be introduced in following sections, in this thesis some state derivatives and constraints will not be represented by linear functions. Since this violates the LQP definition, it poses additional challenges in terms of finding an optimal solution. To express this problem in a general sense the equality and inequality constraints needs to be replaced by some arbitrary functions of the states and control trajectories. Further, in practical applications where samples are obtained at discrete time intervals it is useful to be able to express the optimization problem in discrete time. This is done by partitioning the continuous horizon $\mathbb{H}$ into N discrete values by sampling with interval $\Delta\tau$. Defining $\tau_d(k) = t_0 + k\Delta\tau,\ k \in \{0, 1, \ldots, N-1\}$ yields an expression for the corresponding discrete state vectors $\mathbf{x}_d(k) = \mathbf{x}(\tau_d(k))$ and control vector $\mathbf{u}_d(k) = \mathbf{u}(\tau_d(k))$ over the prediction horizon. For further reference the subscript "d" will be dropped for notational convenience meaning that discrete state vectors and control signals will be referred to as simply $\mathbf{x}(k)$ and $\mathbf{u}(k)$ respectively where k is defined as above. This finally leads to a general and formal definition of the applicable non linear optimal control problem (NLOCP) expressed in discrete time as,

$$\text{Minimize} \quad V(\mathbf{x}(t), \mathbf{u}(0:N-1)) = \sum_{k=0}^{N-1} \mathbf{x}(k)^T\mathbf{Q}(k)\mathbf{x}(k) + \mathbf{u}(k)^T\mathbf{R}(k)\mathbf{u}(k) \tag{2.18a}$$

$$\text{Subject to,} \quad \mathbf{x}(k+1) = f(\mathbf{x}(k), \mathbf{u}(k)) \tag{2.18b}$$

$$g(\mathbf{x}(k), \mathbf{u}(k)) \leq 0 \tag{2.18c}$$

$$\mathbf{x}(0) = \mathbf{x}(t), \quad k = 0, 1, \ldots, N-1 \tag{2.18d}$$

where functions f, g represents the arbitrary constraint functions. Additionally note that, given both cost matrices are positive semi-definite, i.e $\mathbf{Q} \succ 0, \mathbf{R} \succ 0$, the objective function is convex with respect to $\mathbf{x}(k)$ and $\mathbf{u}(k)$ [28].

2.2.1 Solving NLOCPs

The fundamental idea when solving constrained optimization problems is to re-write the problem on an alternate form that is simpler to solve but still returns a solution that is identical or close to the optimal solution of the original problem. Considering now a more general version of problem (2.18) as,

$$\begin{aligned} \text{Minimize,} \quad & V(\mathbf{x}) = f(\mathbf{x}) \\ \text{Subject to,} \quad & g_i(\mathbf{x}) = 0, \quad i = 1, \ldots m \\ & h_j(\mathbf{x}) \leq 0, \quad j = 1, \ldots, p \end{aligned} \tag{2.19}$$

Similarly, $f(\mathbf{x}) \in \mathbb{R}$ represents the objective function to be minimized with $\mathbf{g}(\mathbf{x}) \in \mathbb{R}^m$ and $\mathbf{h}(\mathbf{x}) \in \mathbb{R}^p$ representing the equality and inequality constraints respectively.

Other than assuming smoothness, no other assumptions are made regarding the function's characteristics meaning that they possibly can be non linear. The optimal solution $\mathbf{x}^* \in \mathbb{R}^n$ is further assumed to be a local minimum and regular with corresponding optimal solution $p^* = V(\mathbf{x}^*)$.

To first analyse the inequality constrains $\mathbf{h}(\mathbf{x})$, we can consider an alternative problem $\tilde{V}(\mathbf{x})$ which simply corresponds to $V(\mathbf{x})$ but without the equality constraints $\mathbf{g}(\mathbf{x})$. Similarly, the optimal solution can be denoted as $\tilde{p}^* = \tilde{V}(\mathbf{x}^*)$ One could attempt to instead introduce the inequality constraints in the new objective $\tilde{V}(\mathbf{x})$ together with $f(\mathbf{x})$ and associate positive values with a positive infinitely large cost. However, this would result in a discontinuous and non-differentiable problem which is significantly inconvenient to minimize. Instead, one could relax the constraint and instead introduce a linear cost term as $\mu_j h_j(\mathbf{x})$. With this term it is possible to introduce the Lagrangian,

$$\mathcal{L}(\mathbf{x}, \boldsymbol{\mu}) = f(\mathbf{x}) + \sum_{j=1}^{m} \mu_j h_j(\mathbf{x}) \tag{2.20}$$

where $0 \leq \boldsymbol{\mu} \in \mathbb{R}^p$ represents the so-called Lagrange multipliers. Since these Lagrange variables can tend towards the positive infinity, maximizing the Lagrangian loosely speaking returns the original constrained objective $\tilde{V}(\mathbf{x})$. If the constraints are violated, the Lagrange multipliers would ideally tend towards a relatively large number and would otherwise be set as zero. Formally this means that the original problem formulation can be replaced by,

$$\min_{\mathbf{x}} \max_{\boldsymbol{\mu}} \mathcal{L}(\mathbf{x}, \boldsymbol{\mu}) = \tilde{d}^* \tag{2.21}$$

where $\tilde{d}^*$ represents the corresponding alternative solution to $\tilde{p}^*$ which minimizes the problem $\tilde{V}(\mathbf{x})$. However, since the dual function represents a relaxed version of the original problem, $\tilde{d}^*$ is not necessarily equivalent to $\tilde{p}^*$. Since $\sum_{i=1}^{m} \mu_j h_j(\mathbf{x}) \leq 0$, the solution $\tilde{d}^*$ will instead represent a lower bound of the original problem, i.e $\tilde{d}^* \leq \tilde{p}^*$.

Now introducing the equality constraints $\mathbf{g}(\mathbf{x})$ follows the same reasoning. In this case however, the Lagrange multiplier associated with the equality constraint $\boldsymbol{\lambda} \in \mathbb{R}^m$ is unconstrained since any deviation from $\mathbf{g}(\mathbf{x}) = 0$ should be penalized in the objective. Typically, the order of the two optimizations in Equation (2.21) is also interchanged. This is due to the fact that the Lagrangian, now expressed as $\mathcal{L}(\mathbf{x}, \boldsymbol{\lambda}, \boldsymbol{\mu})$, is concave with respect to the Lagrange multipliers. Due to this, maximizing the Lagrangian will be a convex problem with respect to the Lagrange variables which is much easier to solve than contrary case. Finally, this leads to the dual solution of the original optimization problem $V(\mathbf{x})$ as,

$$d^* = \max_{\boldsymbol{\lambda}, \boldsymbol{\mu}} \min_{\mathbf{x}} \mathcal{L}(\mathbf{x}, \boldsymbol{\lambda}, \boldsymbol{\mu}) = \max_{\boldsymbol{\lambda}, \boldsymbol{\mu}} \min_{\mathbf{x}} f(\mathbf{x}) + \sum_{i=1}^{p} \lambda_i g_i(\mathbf{x}) + \sum_{j=1}^{m} \mu_j h_j(\mathbf{x}) \tag{2.22}$$

where the solution d^* similarly acts as a lower bound on the original solution p^* [29].

Although, $d^* \leq p^*$ also-called weak duality, always holds it is interesting to investigate the case of $d^* = p^*$ also-called strong duality. Assuming that the optimization problem is convex (convex objective, linear inequality constraints and affine equality constraints) and regular it is possible to use the so-called Karush-Kuhn-Tucker (KKT) conditions as necessary and sufficient conditions for optimality. In spite of the fact that the optimization problem in this thesis, does not exhibit these characteristics in general, it is worthwhile to state the conditions in their entirety for future reference. This since they are commonly used in numerical solvers. Given the optimization problem (2.19) with Lagrangian expressed in Equation (2.22), the KKT conditions are stated as follows,

$$\nabla_x \mathcal{L}(\mathbf{x}^*, \boldsymbol{\lambda}^*, \boldsymbol{\mu}^*) = \nabla_x f(\mathbf{x}^*) + \nabla_x \mathbf{g}(\mathbf{x}^*)^T \boldsymbol{\lambda}^* + \nabla_x \mathbf{h}(\mathbf{x}^*)^T \boldsymbol{\mu}^* = 0 \tag{2.23a}$$

$$\mathbf{g}(\mathbf{x}^*) = 0, \tag{2.23b}$$

$$\mathbf{h}(\mathbf{x}^*) \leq 0 \tag{2.23c}$$

$$\boldsymbol{\mu}^* \geq 0 \tag{2.23d}$$

$$\mu_j^* h_j(\mathbf{x}^*) = 0, \quad j = 1, \dots, p \tag{2.23e}$$

Equation (2.23a) states that the minimum of the Lagrangian corresponds to the optimal solution which together with Equation (2.23b) and (2.23c) confirms that the constraints are valid. The Lagrange multipliers associated with the inequality constraints are conditioned in Equations (2.23d) and (2.23e). Here Equation (2.23d) follows the same motivation used when deriving Equation (2.20). The last condition introduced in Equation (2.23e) describes the so-called complementary slackness. If the constraint is strictly active in the optimum, i.e $h_j(\mathbf{x}^*) = 0$, then $\mu_j^* \neq 0$. Conversely if the constraint is inactive $\mu_j^* = 0$. Loosely speaking, if some inequality constraint j is strictly active, it will impact the minimization of the Lagrangian by $\nabla_x h_j(\mathbf{x}^*)\mu_j^*$ which results in an optimum that differs from the one the unconstrained solution obtained from $f(\mathbf{x})$ alone. On the contrary, if said constraint is inactive it will have no impact on the obtained optimum since, $\nabla_x h_j(\mathbf{x})\mu_j = 0$ [30, 31].

2.2.1.1 Sequential Quadratic Programming

As the name suggests, the idea behind the Sequential Quadratic Programming (SQP) method for NLOCPs is to approximate the problem as quadratic, perform a Newton step and then iterate the procedure sequentially until some tolerance is achieved. To illustrate this procedure, lets for now only consider an equality constrained optimization problem,

$$\begin{aligned} \text{Minimize,} \quad & f(x) \\ \text{Subject to,} \quad & g(x) = 0 \end{aligned} \tag{2.24}$$

without any further assumptions regarding the characteristics of $f(x)$ and $g(x)$. This means that the KKT conditions simplify to,

$$\begin{aligned} \nabla_x \mathcal{L}(x^*, \lambda^*) = \nabla_x f(x^*) + \nabla_x g(x^*)^T \lambda^* = 0 \\ g(x^*) = 0 \end{aligned} \tag{2.25}$$

assuming regularity, the above hence represents a system of equations that can be solved for x^*, λ^*.

Since no assumptions have been made regarding the constraints and objective function a suitable general solution is to use the Newton method. Approximating $\nabla_x \mathcal{L}(x, \lambda)$, $g(x)$ using a first-order Taylor series yields,

$$\begin{aligned} \nabla_x \mathcal{L}(x_k + \Delta x, \lambda_k) &\approx \nabla_x \mathcal{L}(x_k, \lambda_k) + \nabla_x^2 \mathcal{L}(x_k, \lambda_k)\Delta x = 0 \\ \nabla_x \mathcal{L}(x_k, \lambda_k + \Delta\lambda) &\approx \nabla_x \mathcal{L}(x_k, \lambda_k) + \nabla_{x,\lambda_k} \mathcal{L}(x_k, \lambda_k)\Delta\lambda = 0 \Rightarrow \\ &\Rightarrow \nabla_x \mathcal{L}(x_k, \lambda_k) + \nabla_x g(x_k)^T \Delta\lambda = 0 \\ g(x_k + \Delta x) &\approx g(x_k) + \nabla_x g(x_k)^T \Delta x = 0 \end{aligned} \tag{2.26}$$

which can be reformulated on matrix form as,

$$\begin{bmatrix} \nabla_x^2 \mathcal{L}(x_k, \lambda_k) & \nabla_x g(x_k)^T \\ \nabla_x g(x_k) & 0 \end{bmatrix} \begin{bmatrix} \Delta x \\ \Delta\lambda \end{bmatrix} = - \begin{bmatrix} \nabla_x \mathcal{L}(x_k, \lambda) \\ g(x_k) \end{bmatrix} \tag{2.27}$$

solving equation system (2.27) hence yields the Newton direction used to update the optimization variables as,

$$\begin{aligned} x_{t+1} &= x_k + \Delta x \\ \lambda_{t+1} &= \lambda_k + \Delta\lambda \end{aligned} \tag{2.28}$$

Further note, if the objective $f(x)$ is quadratic and the constraint $g(x)$ is linear e.g.,

$$\begin{aligned} f(\mathbf{x}) &= \mathbf{x}^T \mathbf{Q}\mathbf{x} + \mathbf{q}^T \mathbf{x}, \quad \mathbf{x}, \mathbf{q} \in \mathbb{R}^n, \mathbf{Q} \in \mathbb{R}^{n \times n} \\ g(\mathbf{x}) &= \mathbf{A}\mathbf{x} + \mathbf{b} = 0, \quad \mathbf{b} \in \mathbb{R}^m, \mathbf{A} \in \mathbb{R}^{m \times n} \end{aligned} \tag{2.29}$$

then, $\nabla_x^2 \mathcal{L}(x_k, \lambda_k) = Q$, $\nabla_x g(x_k) = A$, which can be used to arrive at an explicit solution of problem (2.27).

Using this observation, the entire method can be reformulated as an optimization problem,

$$\begin{aligned} \min_{\mathbf{d}} \ & \mathbf{d}^T \nabla_x^2 f(\mathbf{x}_k)\mathbf{d} + \nabla_x f(\mathbf{x}_k)\mathbf{d} \\ s.t, \ & \nabla_x g(\mathbf{x}_k)\mathbf{d} + g(\mathbf{x}_k) = 0 \end{aligned} \tag{2.30}$$

where $\mathbf{d}$ now represents the Newton search direction for the variable $\mathbf{x}_k$. I.e, on this form, the algorithm is sequentially solving an approximation of the original problem as a quadratic optimization problem.

With the algorithm formulated, lets consider the whole optimization problem as described by Equation (2.19) with both equality and inequality constraints $\mathbf{g}(\mathbf{x})$ and $\mathbf{h}(\mathbf{x})$. With the addition of inequality constraints, all KKT conditions must be considered meaning that it no longer is possible to express the quadratic optimization problem for the Newton direction. This issue is solved by converting the inequality constraints into equality constraints using so-called slack variables. This can be done as follows,

$$\hat{\mathbf{h}}(\mathbf{x}) = \mathbf{h}(\mathbf{x}) + \mathbf{s} \odot \mathbf{s} = 0 \tag{2.31}$$

where $\odot$ indicates element-wise multiplication and $\mathbf{s} \in \mathbb{R}^p$ and are unconstrained. The motivation for squaring the slack variable is to avoid constraining $\mathbf{s}$ to the positive real values and hence avoiding an additional inequality constraint.

The gives the following expression for the Lagrangian,

$$\mathcal{L}(\mathbf{x}, \boldsymbol{\lambda}, \boldsymbol{\mu}, \mathbf{s}) = f(\mathbf{x}) + \mathbf{g}(\mathbf{x})^T \boldsymbol{\lambda} + (\mathbf{h}(\mathbf{x}) + \mathbf{s} \odot \mathbf{s})^T \boldsymbol{\mu} \tag{2.32}$$

However, if one attempts at minimize the above function by computing and setting the derivatives of all respective variables as zero, the complementary slackness condition will appear via,

$$\nabla_s \mathcal{L}(\mathbf{x}, \boldsymbol{\lambda}, \boldsymbol{\mu}, \mathbf{s}) = 2(\mathbf{s} \odot \boldsymbol{\mu}) = 0 \tag{2.33}$$

i.e, for all j either s_j or μ_s is zero. This means that even if the original optimization problem is regular, the resulting system of equations will be underdetermined. One approach, although foolish, is to guess whether either the slack variable or the Lagrange variable is set to zero, however as the number of inequality constraints p grows this quickly becomes practically infeasible. A more reasonable approach is the so-called Active set method, which aims to estimate which of the constraints j are strictly active (i.e, the case when $s_j = 0$). The active set $\mathbb{A}$ hence contains all constraints that are active which are considered as equality constraints, while the rest are, loosely speaking, ignored. Another method, which is particularly popular for large problems, is the interior point method that will be introduced further in the next section [32, 33].

2.2.1.2 Interior Point Method

The principal idea of the interior point method (IPM) is to replace the inequality constraint by introducing a so-called barrier function into the objective function. Typically, the barrier function is chosen as convex according to the following structure,

$$\phi_j(\mathbf{x}) = -\tau \log\Big(-h_j(\mathbf{x})\Big), \quad j = 1, \dots, p \tag{2.34}$$

where $\tau \geq 0$ is a scaling factor and $h_j(\mathbf{x}) \leq 0$ corresponds to the jth inequality constraint. Since the logarithmic function is defined only for strictly positive values and tends to the negative infinity as $h_j(\mathbf{x})$ approaches zero, the objective will tend towards infinity as the inequality constraint is approaching its upper limit. In theory this means that it is possible to represent the inequality constraint together with a convex objective function given that τ is positive and infinitesimally close to zero.

With this addition it is possible to now formulate the optimization problem as,

$$\begin{aligned} \text{Minimize,} \quad & V(\mathbf{x}) = f(\mathbf{x}) - \tau \textstyle\sum_{j=1}^{p} \log\Big(-h_j(\mathbf{x})\Big) \\ \text{Subject to,} \quad & g_i(\mathbf{x}) = 0, \quad i = 1, \dots m \end{aligned} \tag{2.35}$$

with corresponding Lagrangian,

$$\mathcal{L}(\mathbf{x}, \boldsymbol{\lambda}) = f(\mathbf{x}) + \mathbf{g}(\mathbf{x})^T \boldsymbol{\lambda} - \tau \sum_{j=1}^{p} \log\Big(-h_j(\mathbf{x})\Big) \tag{2.36}$$

Hence, the optimization problem is expressed without inequalities which can be solved as introduced in the previous section by specifying the relevant KKT conditions as,

$$\begin{aligned} \nabla_x \mathcal{L}(\mathbf{x}^*, \boldsymbol{\lambda}^*) = \nabla_x f(\mathbf{x}^*) + \nabla_x \mathbf{g}(\mathbf{x}^*)^T \boldsymbol{\lambda}^* + \tau \textstyle\sum_{j=1}^{p} \frac{1}{h_j(\mathbf{x}^*)} \nabla_x h_j(\mathbf{x}^*) = 0 \\ g(\mathbf{x}^*) = 0 \end{aligned} \tag{2.37}$$

Hence in principle, the interior point method utilizes the fundamental SQP approach and relaxes the inequality constraint by introducing barrier functions in the objective [34].

Note however that the derivative of the barrier function introduces the term $\frac{1}{h_j(\mathbf{x})}$ into the KKT conditions. If the inequality constraints come closer to being activated, i.e $h_j(\mathbf{x}) \to 0$, this potentially introduces numerical issues for the Newton method. This issue can be accounted for by utilizing the so-called primal-dual interior point method. Defining,

$$\mu_j = \tau \frac{1}{h_j(\mathbf{x})} \tag{2.38}$$

it becomes possible to re-write the KKT conditions as,

$$\begin{aligned} \nabla_x \mathcal{L}(\mathbf{x}^*, \boldsymbol{\lambda}^*) = \nabla_x f(\mathbf{x}^*) + \nabla_x \mathbf{g}(\mathbf{x}^*)^T \boldsymbol{\lambda}^* + \textstyle\sum_{j=1}^{p} \mu_j \nabla_x h_j(\mathbf{x}^*) = 0 \\ g(\mathbf{x}^*) = 0 \\ h(\mathbf{x}^*) + \mathbf{s} = 0 \\ \mu_j s_j = \tau, \quad j = 1, \ldots, p \\ \boldsymbol{\mu} > 0, \mathbf{s} > 0 \end{aligned} \tag{2.39}$$

which is avoids the mentioned numerical issues. Do note that this approach introduces inequality constraints on $\boldsymbol{\mu}$ and $\mathbf{s}$. These conditions can however be ensured using backtracking which is not difficult in practice [35].

2.3 Predictive Propulsion Control

The Cambridge English dictionary defines propulsion as "*The force produced by a system for moving a vehicle or other object*". In this context, the concept of predictive propulsion control refers to control methods that aim to find a suitable force for moving the vehicle, utilizing a prediction of the vehicle system over a certain future time or distance. In practice, this is typically associated with optimizing the vehicle in some aspect, such as e.g., energy efficiency, which also is one of the most attractive advantages of this method. Another considerable advantage is the ability to formulate constraints on certain variables in the system model. This means that it is, in many cases, possible to ensure that the system prediction represents a feasible solution for the real-life system. Both points are not typically achievable using conventional methods for set-point tracking, such as e.g., a PID controller. However, they do also require a substantially larger amount of computation power which has been one of the main limiting factors for practical applications.

2.3.1 Predictive Eco-Driving

Eco-driving is an approach that aims to minimize the energy consumption by propelling the vehicle in a more efficient manner. In its most basic form, this approach considers the inclination of the future terrain to efficiently utilize the kinetic and potential energy currently "stored" in the vehicle. In practice, the least energy efficient operation typical relates to sharp accelerations and braking. This means that the most energy efficient solution typically corresponds to minimizing the acceleration and braking based on the knowledge of the future inclination. This typically also amounts to a somewhat slower average velocity of the vehicle [36]. One of the first papers published using this approach considers an ICEV with a corresponding propulsion and fuel efficiency model together with information about the future inclination. This article constructs a force balance over the vehicle, like what is seen in Equation (2.1) and expresses the fuel consumption $f_c(t)$ via a polynomial regression based on the vehicle velocity $\dot{x}(t)$ as,

$$f_c(t) = \sum_i \beta_i \dot{x}(t)^i \tag{2.40}$$

This term is then minimized to find an optimal velocity $\dot{x}(t)$ over the entire horizon. This approach was evaluated in a simple simulation with an altitude difference of 19m and showed a decrease in fuel consumption by upwards of $\sim$ 7% [37]. The same methodology can be applied in the case of a BEV by interchanging the fuel efficiency model with an energy efficiency model as illustrated in [38]. Considering that the energy storage unit now consists of a battery it is instead appropriate to minimize the instantaneous battery power usage. As seen in Equation (2.5a) and further Equation (2.7) the battery usage can directly be related to the motor force demand which allows the energy usage to be minimized by in a similar fashion as for the ICEV case.

In more recent years, more accurate strategies have been developed for a wide array of configurations for ICEV, FCHEV and BEV. One key addition has been to utilize the torque $\mathcal{T}(t)$ and angular velocity $\omega(t)$ which can be expressed based on the vehicle velocity and wheel force. This can be done as,

$$\omega(t) = \frac{R(\gamma)}{r_{whl}} v(t) \quad \mathcal{T}(t) = \frac{1}{R(\gamma)} F_{EM,whl}(t) \tag{2.41}$$

where $R(\gamma)$ represents the gear ratio as a function of the gear $\gamma \in \mathbb{N}$ and r_{whl} represents the wheel radius. The product of the motor angular velocity and torque can then be used to predict the power output. This is e.g., being used in current state-of-the art models to obtain more accurate predictions of the motor energy/fuel usage [39, 40]. However, this introduces an additional optimization variable γ that only takes integer values. As introduced in section 2.2.1 the SQP and further the IPM both really on computing the continuous derivatives of the Lagrangian, which naturally pose issues since the gears are discrete values. This means that the optimization of the gears, also referred to as gear scheduling, needs to be solved using a different method, e.g., dynamic programming.

2.3.2 Control Architectures

The most straight forward approach for optimizing with respect to both the continuous velocity and the discrete gear could be considered as solving the entire problem simultaneously using a single program. Since methods that are applicable for integer values, e.g. dynamic programming, typically deal with entirely discrete systems it becomes necessary to also treat the velocity as a discrete state. This is done by partitioning the velocity $v(t)$ into discrete values $v(i) = v_{min} + i\Delta v,\ i = 0, \dots, M_g - 1$ within some feasible range $\mathbb{V} \in [v_{min}, v_{max}]$ where the resolution is described by $\Delta v = (v_{max} - v_{min})/M_v$. The same principle can be applied to the gears with corresponding range $\mathbb{G}$ and discrete values M_g. As the resolution increases the returned solution for the velocity will naturally be more accurate, however the computational complexity will also significantly grow. This incentivises the use of a so-called, pre-filter, that uses heuristic laws to select a small $\mathbb{V}$ and $\mathbb{G}$ which can have a relatively high resolution and still utilize a relatively small number of discrete values. This control architecture is illustrated below in Figure 2.9.

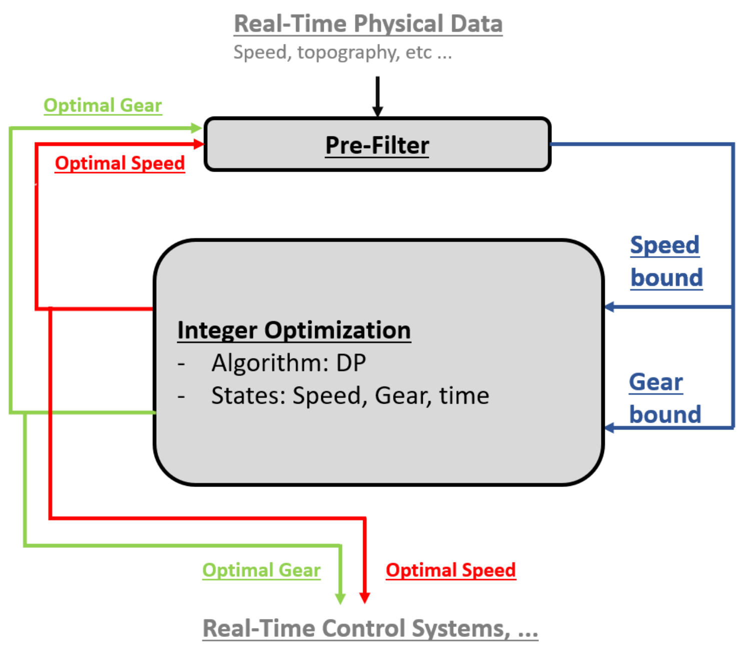

Figure 2.9: A single-solver solution for optimizing energy efficiency with respect to both velocity and gear.

Although practical, discretising continuous optimization variables generally leads to a less accurate solution. Additionally, this method also lacks the rigorous mathematical interpretation that is provided by the KKT conditions. An alternative approach is to instead decouple the optimization, i.e solving the optimization problem with respect to the continuous and discrete variables separately. In this case, the continuous problem for the velocity can be solved using QP methods while the gear scheduling can be solved by a DP. The two separate problems are hence solved sequentially. First, an optimal velocity is obtained assuming that the gears are fixed at the corresponding values found by the previous solution of the gear scheduling optimization problem. Similarly, the gear scheduling optimization problem assumes that the vehicle speed is kept at the optimal solution obtained by the QP solver. A schematic illustration of the control architecture is shown below in Figure 2.10

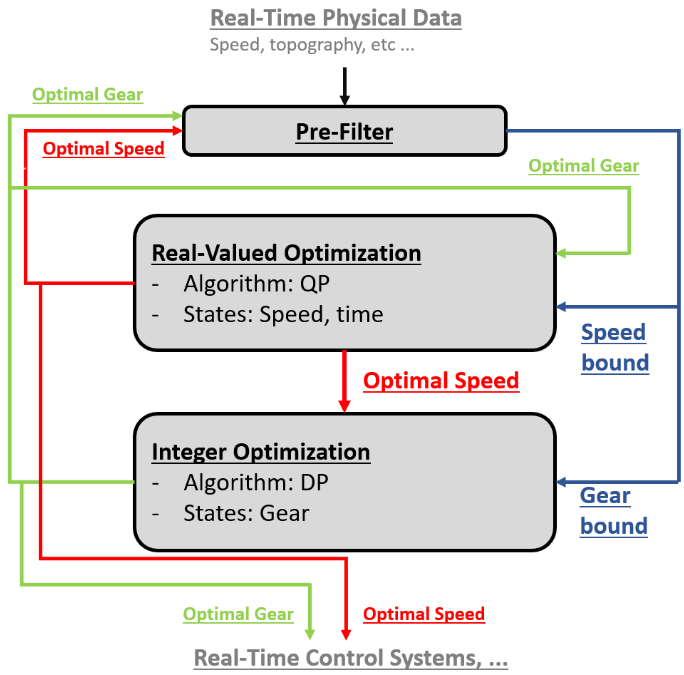

Figure 2.10: A dual-solver solution for optimizing energy efficiency with respect to velocity and gear separately, simplified and adapted from [41].

Note that the pre-filter is being utilized also in this case to decrease the computational complexity [41].

The pre-filter does in this case compute the reference for the QP solver which can be summarized in algorithm 1 below. The principal idea is to track the speed limit if it is feasible in terms of the available engine power. The algorithm is initialized with the current velocity at time t and then calculates the feasible velocities in a forward pass over the horizon. The idea then is that this “controller” takes one of 2 decisions, speed up with maximum power or brake with maximum power. To keep track of these decision one can define a “decision log ” D_{log} that consists of a vector with the same size as the amount of steps in the horizon. The algorithm returns $\mathbb{V}$ which represents the velocity bound at each step k over the horizon. This is based on an allowed maximum deviation $\Delta v_{min}, \Delta v_{max}$ from the obtained reference V_{log}.

Algorithm 1 Simplified Pre-filter algorithm

Initilize $D_{log} = [], V_{log} =$ zeros(N,1), $V_{log}(1) = v_0$
for Steps (k) in horizon $\mathbb{H}_d$ **do**
  if $v(k-1) \leq v_{limit}(k)$ **then**
    $D_{log}(k) =$ “*Speed up*”
    Find max EM power: $(P_{EM}^{max}(k))$
    Find max speed: $(v_{max}(k))$
    Filter if above reference: $V_{log}(k) = min\{v_{max}(k), v_{limit}(k)\}$
  else if $v(k-1) > v_{limit}(k)$ **then**
    $D_{log}(k) =$ “*Brake*”
    Brake to reach speed limit: $V_{log}(k) = v_{limit}(k)$
  end if
end for
$V_{min} = V_{log} - \Delta v_{min}$
$V_{max} = V_{log} + \Delta v_{max}$
return $\mathbb{V} = \begin{bmatrix} V_{min} \\ V_{max} \end{bmatrix}$

3
Problem Formulations

This section aims at introducing the optimization problems on a conceptual form to aid the reader in upcoming sections. Notable adaptations to the optimization problem (e.g., variable swaps) and physical modelling are introduced in the methods section. Both optimization problems are stated with mathematical rigour in Appendix A.1 and A.2.

3.1 Safe Braking

The optimization problem was solved by expressing the horizon over position s, as opposed to time t. By discretising the horizon $\mathbb{H}_s \in [s_0, s_f]$ introducing $s(k) = s_0 + k\Delta s, k = 0, \ldots, N-1,\ s_f = s_0 + (N-1)\Delta s$ the problem can also be expressed in discrete intervals. The state corresponding to the vehicle velocity was also reformulated as kinetic energy via the fundamental relation,

$$E_k(s(k)) = \frac{m_v v(s(k))^2}{2} \tag{3.1}$$

Note that, to simplify notation, all variables depending on the position "$\bullet(s(k))$" will further be referred to as simply "$\bullet(k)$".

Hence, the discrete states $\mathbf{x}(k)$ includes the kinetic energy of the vehicle and the brake temperature $T_{brake}(k)$,

$$\mathbf{x}(k) = \begin{bmatrix} x_1(k) \\ x_2(k) \end{bmatrix} = \begin{bmatrix} E_k(k) \\ T_{brake}(k) \end{bmatrix} \tag{3.2}$$

with corresponding control signals $\mathbf{u}(k)$ containing the electric motor force at the wheels $F_{EM,whl}(k)$ and the mechanical brake force $F_{brake}(k)$.

$$\mathbf{u}(k) = \begin{bmatrix} u_1(k) \\ u_2(k) \end{bmatrix} = \begin{bmatrix} F_{EM,whl}(k) \\ F_{brake}(k) \end{bmatrix} \tag{3.3}$$

Two slack variables where further defined based on the vehicle kinetic energy as,

$$\begin{aligned} E_k(k) &\leq E_{ref}(k) + \delta_1(k) \\ E_k(k) &\geq E_{ref}(k) - \delta_2(k) \end{aligned} \tag{3.4}$$

where $E_{ref}(k)$ corresponds to the kinetic energy of the vehicle at the maximum allowed velocity of the vehicle. This approach was taken to be able to introduce an asymmetrical cost on deviations from the reference. Too high speeds should always be avoided but low speeds are sometimes necessary. Additionally three different slack variables where associated with three different brake temperature levels,

$$\begin{aligned} T_{brake}(k) &\leq 300\text{C}^\circ + \delta_3(k) \\ T_{brake}(k) &\leq 350\text{C}^\circ + \delta_4(k) \\ T_{brake}(k) &\leq 550\text{C}^\circ + \delta_5(k) \end{aligned} \tag{3.5}$$

This was done to be able to tune the "Brake Temperature-Speed" trade-off more accurately.

The equality constraints can simply be summarized as to describe the dynamics of the two states,

$$\mathbf{g}(\mathbf{x}(k), \mathbf{u}(k), \mathbf{P}(s_0)) = \mathbf{x}(k+1) \in \mathbb{R}^2 \tag{3.6}$$

where $\mathbf{P}(s_0)$ represents a matrix of constants dependant on the initial position of the horizon s_0.

The inequality constraints are generally defined to ensure that physical limitations of the system are not violated. For the electric motor this means limiting the maximum force based on internal dimensioning $F_{EM}^{max}(\mathbf{x}(k), \mathbf{P}(s_0))$, the maximum supplied and withdrawn battery power $F_{bat}^{max}(\mathbf{x}(k), \mathbf{P}(s_0)), F_{bat}^{min}(\mathbf{x}(k), \mathbf{P}(s_0))$ and driver comfort $F_{EM,c}^{max}(\mathbf{x}(k), \mathbf{P}(s_0))$. The brake system similarly has a comfort constraint $F_{brake,c}^{max}(\mathbf{x}(k), \mathbf{P}(s_0))$ and the kinetic energy is constrained based on a minimum allowed velocity E_{min}. This amounts to the following constraints,

$$\begin{aligned} u_1(k) &\leq F_{EM}^{max}(\mathbf{x}(k), \mathbf{P}(s_0)) \\ u_1(k) &\leq F_{bat}^{max}(\mathbf{x}(k), \mathbf{P}(s_0)) \\ u_1(k) &\geq F_{bat}^{min}(\mathbf{x}(k), \mathbf{P}(s_0)) \\ u_1(k) &\leq F_{EM,c}^{max}(\mathbf{x}(k), \mathbf{P}(s_0)) \\ u_2(k) &\leq F_{brake,c}^{max}(\mathbf{x}(k), \mathbf{P}(s_0)) \\ x_1(k) &\geq E_{min} \end{aligned} \tag{3.7}$$

which with minor modifications can be reformulated into a single vector function,

$$\mathbf{h}(\mathbf{x}(k), \mathbf{u}(k), \mathbf{P}(s_0)) \leq 0 \tag{3.8}$$

Finally, combining the above it becomes possible to express the optimization problem in a familiar form,

$$\begin{aligned} \text{Minimize,} \quad & \sum_{k=0}^{N-1} \boldsymbol{\delta}(k)^T \mathbf{Q} \boldsymbol{\delta}(k) + \sum_{k=0}^{N-2} + r_0 u_2(k)^2 && \text{(3.9a)} \\ \text{Subject to,} \quad & \mathbf{g}(\mathbf{x}(k), \mathbf{u}(k), \mathbf{P}(s_0)) - \mathbf{x}(k+1) = 0 && \text{(3.9b)} \\ & \mathbf{h}(\mathbf{x}(k), \mathbf{u}(k), \mathbf{P}(s_0)) \leq 0 && \text{(3.9c)} \\ & \mathbf{x}(0) = \mathbf{x}_0, \; k = 1, \ldots, N-2 && \text{(3.9d)} \end{aligned}$$

with $\mathbf{Q} \in \mathbb{R}^{5\times5}$ representing a diagonal cost matrix, r_0 representing a scalar cost and $\mathbf{x}(k) \in \mathbb{R}^2$, $\mathbf{u}(k) \in \mathbb{R}^2$ with $\boldsymbol{\delta}(k) \in \mathbb{R}^5$.

3.2 Safe Braking and Propulsion

Now introducing the 2 electric motors in the optimization problem. Since the gear scheduling problem can return vastly different gears for the respective motors it becomes necessary to model both electric motors temperature separately. This introduces 2 more states,

$$\begin{aligned} x_3(k) &= T_{EM,1}(k) \\ x_4(k) &= T_{EM,2}(k) \end{aligned} \tag{3.10}$$

which are appended to the complete state vector $\mathbf{x}(k)$.

No additional control signals were added but 2 new slack variables where added in association to the new EM temperatures,

$$\begin{aligned} T_{EM,1}(k) &\leq 170\text{C}^\circ + \delta_6(k) \\ T_{EM,2}(k) &\leq 170\text{C}^\circ + \delta_7(k) \end{aligned} \tag{3.11}$$

these where similarly appended to the complete slack variable vector $\boldsymbol{\delta}(k)$.

In terms of constraint, 2 equality constraints where natural introduced to describe the update equations of the EM temperature models. For notational purposes this update equation can now be defined as,

$$\hat{\mathbf{g}}(\mathbf{x}(k), \mathbf{u}(k), \mathbf{P}(s_0)) = \mathbf{x}(k+1) \in \mathbb{R}^2 \tag{3.12}$$

One additional constraint was also added in an attempt to limit the change of the engine force at high temperatures. This was expressed as,

$$u_1(k) - \Delta_F(x_3(k), x_4(k)) \leq u_1(k+1) \leq u_1(k) + \Delta_F(x_3(k), x_4(k)) \tag{3.13}$$

with $\Delta_F(x_3(k), x_4(k))$ representing a temperature dependant scalar. This can similarly be rewritten to on the more convenient form,

$$\hat{\mathbf{h}}(\mathbf{x}(k), \mathbf{u}(k), \mathbf{P}(s_0)) \leq 0 \tag{3.14}$$

which finally gives the complete optimization problem on an almost identical form,

$$\begin{aligned} \text{Minimize,} \quad & \sum_{k=0}^{N-1} \boldsymbol{\delta}(k)^T \mathbf{Q} \boldsymbol{\delta}(k) + \sum_{k=0}^{N-2} r_0 u_2(k)^2 && \text{(3.15a)} \\ \text{Subject to,} \quad & \mathbf{g}(\mathbf{x}(k), \mathbf{u}(k), \mathbf{P}(s_0)) - \mathbf{x}(k+1) = 0 && \text{(3.15b)} \\ & \mathbf{h}(\mathbf{x}(k), \mathbf{u}(k), \mathbf{P}(s_0)) \leq 0 && \text{(3.15c)} \\ & \mathbf{x}(0) = \mathbf{x}_0, \ k = 1, \ldots, N-2 && \text{(3.15d)} \end{aligned}$$

now with $\mathbf{Q} \in \mathbb{R}^{7\times 7}$ representing a diagonal cost matrix, r_0 representing a scalar cost and $\mathbf{x}(k) \in \mathbb{R}^4$, $\mathbf{u}(k) \in \mathbb{R}^2$ with $\boldsymbol{\delta}(k) \in \mathbb{R}^7$.

4
Methods

This section outlines the methods used for physical modelling, optimization formulation and solving. The “novel” system models were derived based on fundamental physical relations and discussions with the representatives at Volvo. Note that some details have been excluded due to confidentiality. Formal derivations of the mathematical models are displayed in Appendix A.3, A.4 and A.5.

The main software that was used in this thesis was Matlab and Simulink (version 2017b). Although different openly distributed optimization solvers were tested through out the thesis (e.g, Acados) the final version uses the Casadi software running the IpOpt solver. This tool aims at solving problems that e.g, are specified on the form of Equation (2.18) [42, 43].

The principle idea for obtaining a safe and energy efficient controller in this thesis is to introduce an additional optimization problem that replaces the pre-filter in the control architectures that were introduced in Section 2.3.2. The objective of this controller will be to suggest a maximum allowed velocity that ensures that the safety conditions of the investigated components are kept. The underlying controller will then optimize the energy efficiency with respect to gears and allowed velocities. This controller was provided by Volvo. To investigate the impact of the additional layer, 3 different controller structures were compared,

- The conventional controller that does not utilize any predictive information, henceforth referenced to as “Static”.
- The current predictive controller, henceforth referenced to as “PEM”.
- The current predictive controller with the “Safe” pre-filter addition, henceforth referenced to as “Safe-PEM”.

Additionally, an improved heuristic pre-filter was introduced in an attempt to obtain a more computationally efficient solution. This adds one more case,

- The current predictive controller with an improved “safe” pre-filter, henceforth referenced to as “Heur-PEM”.

Within the “Safe-PEM”approach several different methods were tested. Since decreasing the brake temperature typically amounts to decreasing the speed, three different tunings of the cost matrix $\mathbf{Q}$ were investigated. These are summarized shortly in the table 4.1 below,

Table 4.1: Key details concerning the different cost matrix tuning.

	Objective
Conservative	Keep temperature below 350^C
Medium	Moderately exceed 350^C
Aggressive	Keep temperature below 550^C

This was obtained by tuning q_{33}, q_{44} and q_{55} corresponding to costs for brake temperatures above $300, 350$ and $550\ °C$ respectively. The problem formulation for this controller is described in Section 3.1 Further, to investigate optimal derate strategies for the EMs, this problem is extended to include the EM temperature, as described in Section 3.2. This can be considered to have two main objectives.

- Decrease time spent at high temperatures, defined as above $165C°$, and never exceed $180°C$, defined as the "critical temperature".
- When derating the EM, avoid sharp drops in power.

The performance of each controller was then evaluated for three different cycles and two different weights (46 and 64 tons) which was carried out in a simulation tool that was provided by Volvo. Some key characteristics of the cycles are included in the table 4.2 below.

Table 4.2: Some key characteristics of the 3 investigated cycles.

	"Difficulty"	Length (km)	Highest vs lowest elevation (m)
Cycle 1	Easy	85	122
Cycle 2	Medium	363	425
Cycle 3	Hard	258	817

All cycles were also assumed to have a constant reference speed limit at 80 km/h.

4.1 Optimization Solver

Casadi provides an interface that allows the user to define the system dynamics and constraints using symbolic expressions. Since Casadi uses so-called algorithmic differentiation, all functions need to be continuous. In this case, since the system dynamics were based on continuous physical models, they were also specified using continuous dynamics. Since the tool aims at solving discrete optimization problems like (2.18), these equations were integrated using the fourth order Runge Kutta method (RK4). The IpOpt solver utilizes the interior point method that was introduced in Section 2.2.1 [44].

4.1.1 Problem Adaptations

One goal when formulating the optimization problem is to avoid non linear constraint in favour of linear whenever possible. This is since, as introduced in sections 2.2.1, SQP problems become easier to solve and can be interpreted using rigorous mathematical conditions. One key motivation for defining the problem over a horizon basted on distance rather than a horizon based on time is dealing with e.g., the road inclination $\alpha(s)$ which naturally depend on the current position s. If the horizon were to be based on time this would require an interpolation based on the sampled elevation data, which would lead to a more involved function. If instead considering distance, it becomes possible to sample the inclination at all points $s(k)$ over the horizon and simply introduce these as parameters in Equation (2.1), effectively avoiding a potentially non linear function. A similar result is obtained when considering potential changes in the speed limit. Worth noting is that it is still possible to consider time, as e.g. was done in the "founding paper" of the eco-driving approach [37]. However, as will be introduced further, it can be significantly advantageous in terms of computational complexity to instead consider distance. One notable impact of the variable change is on the system dynamics. Via the chain rule,

$$\frac{\partial \mathbf{x}(t)}{\partial t} = \frac{\partial \mathbf{x}(s)}{\partial s}\frac{\partial s}{\partial t} = \frac{\partial \mathbf{x}(s)}{\partial s} v(s) \tag{4.1}$$

meaning that the velocity will be introduced in all state update equations.

As a consequence, further simplifications can be made to the state update equations. The force balance as introduced in Equation (2.1) can be rewritten in terms of kinetic energy as,

$$\frac{\partial E_k(s)}{\partial s} = F_{EM,whl}(s) + F_{brake}(s) - \frac{C_d A_p \rho E_k(s)}{m} - m_v g(c_r \cos(\alpha(s)) + \sin(\alpha(s)) \tag{4.2}$$

which yields a linear update equation and loosely speaking a more "well behaved" solution to the optimization problem.

4.2 Brake Temperature Modelling

The dynamics of the brake temperature $T_{brake}(s)$ was formulated by constructing a heat balance over each disc, initially expressed in time. By assuming that all 6 brake system on the truck experience the same load, a heat balance for each disc can be written on conceptual form as,

$$\frac{\partial}{\partial t}\left(H_{internal}(t)\right) = \frac{1}{n_{truck}}\left(H_{in}(t) - H_{out}(t)\right) \tag{4.3}$$

where n_{truck} represents the number of wheels on the truck. As previously introduced in Section 2.1.4, only the truck brake temperature was considered.

Each term in the conceptual balance was then expressed based on physical knowledge of the brake system. The total input heat $H_{in}(s)$ was assumed to equal the power that was consumed by the brake pads, i.e $P_{brake}(t) = F_{brake}(t)v(t)$. With the truck brake force expressed by Equation (2.12) the total input heat to the truck brake discs could be modelled as,

$$H_{in}(t) = F_{brake}(t)v(t) \tag{4.4}$$

where potential model inaccuracies due to force losses in the brake system were neglected. As a note on implementation, Equation (2.12) is discontinuous due to the use of the "min" function. This meant that the relation for the brake force had to be approximated with a smooth function which resulted in an over estimation of the brake force and non linear dynamics with respect to the input signals.

The brake discs heat output $H_{out}(t)$ was considered to be described by cooling that occurs due to convective heat transfer between the pads and the surrounding air. This means that the total heat output of the discs could be described by,

$$H_{out}(t) = n_{truck} A_d h_{brake}\Big(T_{brake}(t)\Big)(T_{brake}(t) - T_{amb}) \tag{4.5}$$

where A_p represents the exposed surface area of the a disc, $h_{brake}(T_{brake}(t))$ represents a temperature dependant heat transfer coefficient and T_{amb} represents the ambient temperature. This notably introduces a non linear relation in the dynamics [45].

Lastly, the internal heat of each brake pad was modelled as,

$$H_{internal}(t) = m_{disc} C_{p,brake}(t) T_{brake}(t) \tag{4.6}$$

with the specific heat capacity $C_{p,brake}(t)$ described as a linear function of the brake temperature,

$$C_{p,brake}(t) = \xi_0 + \xi_1 T_{brake}(t) \tag{4.7}$$

which was derived by fitting $\boldsymbol{\xi}$ to data.

Using the above relation, it was then possible to formulate the change in temperature depending on positions as,

$$\frac{\partial T_{brake}(s)}{\partial s} = \frac{m_{disc}^{-1}}{\xi_0 + 2\xi_1 T_{brake}(s)} \left(\frac{1}{n_{truck}} F_{truck}(s) - \frac{1}{v(s)} A_d h\big(T_{brake}(t)\big)(T_{brake}(s) - T_{amb}) \right) \tag{4.8}$$

4.3 Electric Motor Temperature Modelling

The dynamics of the EM winding temperatures was derived in a similar fashion by constructing a heat balance, in this instance over each motor $i = 1, 2$,

$$\frac{\partial}{\partial t}\left(H_{internal,i}(t)\right) = \left(H_{in,i}(t) - H_{out,i}(t)\right) \tag{4.9}$$

In this case the input heat to each motor $H_{in,i}(t)$ was model based on the total heat losses of the motor $P_{EMi,loss}(t)$. This was done by fitting a function of the torque

$\mathcal{T}_{EMi}(t)$ and angular velocity $\omega_{EMi}(t)$ which, in turn can be expressed based on the vehicle velocity and wheel force. The power losses were predicted as,

$$H_{in,i}(t) = P_{Heat,EM}(s) = \sigma_0 \omega_{EMi}(s) + \sigma_1 \omega_{EMi}^2(s) + \sigma_2 \mathcal{T}_{EMi}^2(s) + \sigma_3 \mathcal{T}_{EMi}^4(s) \quad (4.10)$$

where $\boldsymbol{\sigma}$ represents the coefficients fitted to data and with corresponding expression for the torque and angular velocity as,

$$\omega_{EMi}(t) = \frac{R(\gamma_i(t_0))}{r_{whl}} v(t) \quad \mathcal{T}_{EMi}(t) = \frac{1}{R(\gamma_i(t_0))} F_{EM,whl}(t), i = 1, 2 \quad (4.11)$$

Note that this introduces the discrete valued gears γ into the optimization. To avoid solving a mixed integer problem, these were assumed as constants and set according to the last solution of the underlying DP at time t_0.

The heat output was in a similar fashion modelled as convective heat transfer between the motor windings and the surrounding air. This can similarly be explained as,

$$H_{out}(t) = A_{EM} h_{EM} (T_{EMi}(t) - T_{amb}) \quad (4.12)$$

where A_{EM} represents the effective area and h_{EM} represents the heat transfer coefficient. Note that the heat transfer coefficient in this case is not assumed to be temperature dependant.

Lastly, the internal heat of the respective motor was described in a similar fashion,

$$H_{internal}(t) = m_{EMi} C_{p,EM} T_{EMi}(t) \quad (4.13)$$

note that the specific heat capacity $C_{p,EM}$ is not assumed to be temperature dependant.

4.3.1 Adaptive Parameter Estimation

Due to a lack of data, it was not possible to estimate a temperature dependant specific heat capacity and heat transfer coefficient, as was possible for the brake temperature case. It was similarly only possible to estimate the total motor losses and not the ones corresponding only to the EM windings. To account for modelling inaccuracies due to these factors, different adaptive models were tested. These were implemented using an extended kalman filter (EKF). The final version utilizes two parameters β_0, β_1 that represent modelling deviations in the input and output heat respectively.

With minor modifications this, finally leads to the formulation of the EM temperature dynamics,

$$\frac{\partial T_{EMi}(s)}{\partial s} = \frac{1}{v(s)} \left(\beta_0(s_0) P_{EM,loss}(\omega_{EMi}(s), \mathcal{T}_{EMi}(s)) + \beta_1(s_0)(T_{EMi}(t) - T_{amb})\right) \quad (4.14)$$

with $\boldsymbol{\beta}(s_0)$ being updated based on temperature measurements at distance s_0. The adaptive parameters were notably initialized as,

$$\boldsymbol{\beta}(0) = \begin{bmatrix} \frac{1}{m_{EMi} C_{p,EM}} \\ \frac{A_{EM} h_{EM}}{m_{EMi} C_{p,EM}} \end{bmatrix} \quad (4.15)$$

4.4 Heuristic Pre-Filter Approach

This approach serves as an extension of the existing pre-filter algorithm described in Section 2.3.2. The idea in this case is to additionally predict the brake and EM temperatures that would result from the suggested velocity reference. If the predicted temperatures exceed allowed limits at some step k^* then the algorithm would go through the decision log $D_{log}(1:k^*)$ and changes the latest "Speed Up" decision to instead brake only with the electric motor ("EM Brake")s. This ideally lowers the power demand on the brake and motor system leading up to step k^*, which decreases the temperatures. This fundamental principal is illustrated in algorithm 2 below. Notably, this algorithm no longer computes a single forward-pass, which increases the computational complexity.

Algorithm 2 Fundamental principle of the "safe" pre-filter algorithm.

Initilize $V_{log} = \text{zeros}(N,1)$, $V_{log}(1) = v_0$
for Steps (k) in horizon $\mathbb{H}_d$ **do**
  Use Algorithm 1 to find $V_{log}(k)$
  Calculate temperatures $T_{brake}(k), T_{EM1}(k), T_{EM2}(k)$
  if Temperature constraint is violated **then**
    In $D_{log}(1:k^*)$ *find latest* "Speed up" $=\ \hat{k}$
    Set $D_{log}(\hat{k})$ = "EM Brake"
    Set $k = \hat{k}$
  end if
end for
$V_{min} = V_{log} - \Delta v_{min}$
$V_{max} = V_{log} + \Delta v_{max}$
return $\mathbb{V} = \begin{bmatrix} V_{min} \\ V_{max} \end{bmatrix}$

Based on the problem formulations introduced in sections 3.1 and 3.2 the objective of this algorithm was to maintain a brake temperature below 350 C^o, maintain an EM temp below 180 C^o and achieve a smooth derate of the motor power.

5

Results

This section outlines the results of the three main problems. The results are initially presented separately but are all compared together in the final section. Sections 5.1, 5.2 and 5.3 aim to introduce the controller behavior in a more qualitative fashion while section 5.4 compares all controllers quantitatively. Again, some results have been omitted or reformulated because of confidentiality. Additional results, not referenced in following sections are displayed in Appendix B.

5.1 Safe Braking

This section outlines the result obtained when solving the optimal control problem introduced in section 3.1. Figure 5.1 visualizes a comparison between the PEM controller and the most conservative Safe-PEM controller. In this case the brake temperature and speed has been plotted for a particularly challenging section of cycle 3 using a 64 ton vehicle.

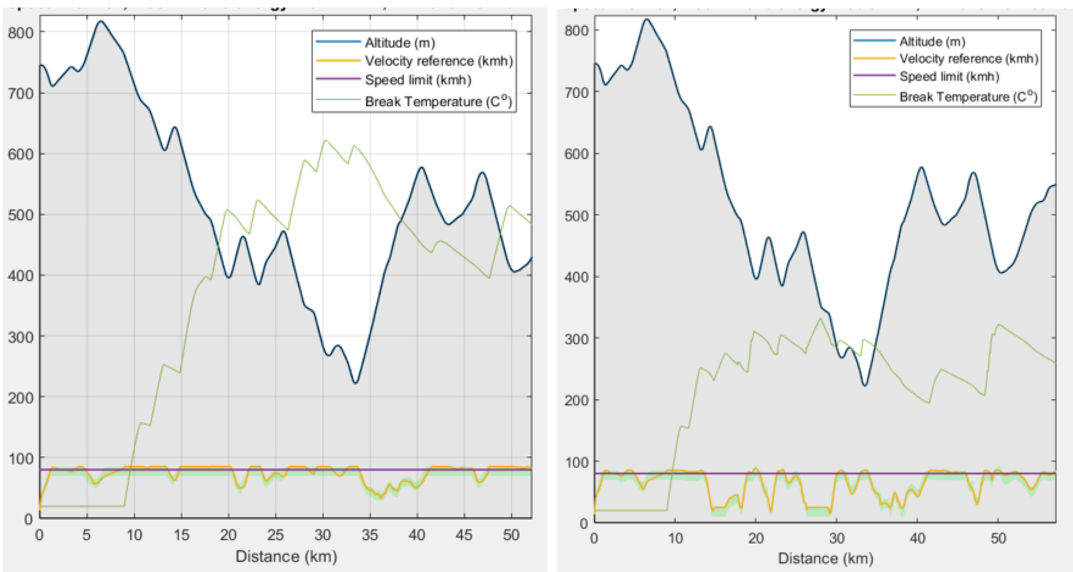

(a) Performance of the PEM controller for a section of cycle 3 and a 64 ton vehicle.

(b) Performance of the Conservative Safe-PEM controller for a section of cycle 3 and a 64 ton vehicle.

Figure 5.1: Comparison between the original predictive controller and the most conservative safe controller.

The 3 different tunings of the Safe-PEM controller are further compared below in Figure 5.2, also for a section of cycle 3 and a 64 ton vehicle.

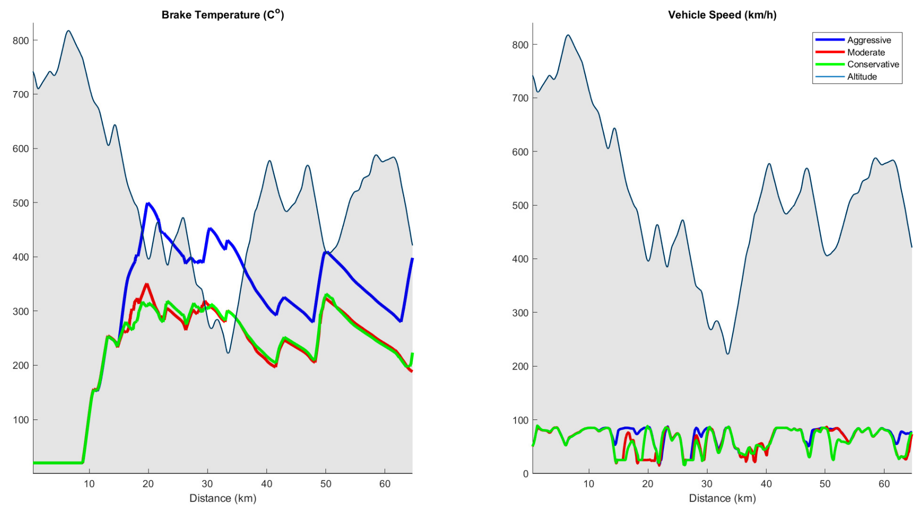

Figure 5.2: A comparison between the 3 different tunings of the Safe-PEM controller, in terms of speed and brake temperature. Evaluated for a section of the cycle 3 and a 64 ton vehicle.

5.2 Safe Braking and Propulsion

This section outlines the results for the optimal control problem described in section 3.2. Figure 5.3 visualizes a comparison in terms of temperature between different derate strategies for one of EM. This includes the cases where the EM is not derated at all (noted “None”), EM derate according to heuristic laws (noted “Heur”) and finally EM derate based on solving an optimal control problem (noted “MPC”). The case displayed in the Figure is for section of cycle 3 and a 64 ton vehicle.

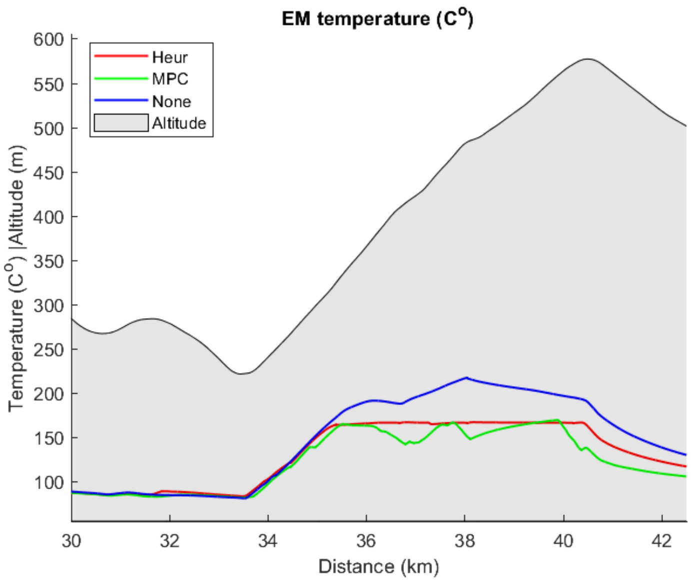

Figure 5.3: Comparison between different derate strategies based on their impact on the temperature profile for EM 1. The studied case is a section of cycle 3 with a 64 ton vehicle.

Further, Figure 5.4 visualises a comparison of the exact same case as above but now for the power constraint on the EM. Note that the values are normalized based on the maximum allowed EM power, based in turn on physical limitations.

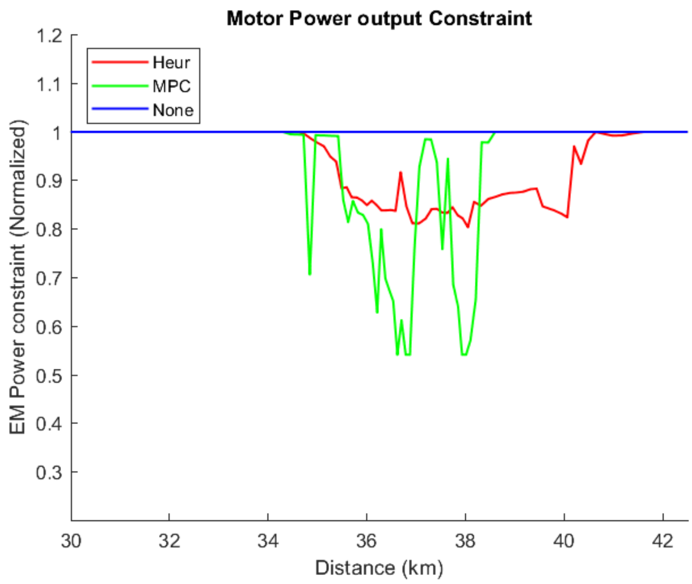

Figure 5.4: Comparison between different EM derate strategies based on the power constraints on EM1. The studied case is a section of cycle 3 with a 64 ton vehicle.

5.3 Heuristic Pre-filter

This section outlines the results obtained when utilizing the altered pre-filter algorithm i.e, without introducing any additional optimal control problem. Figure 5.5 displays a comparison between the PEM and Heur-PEM controllers in terms of brake temperature and speed.

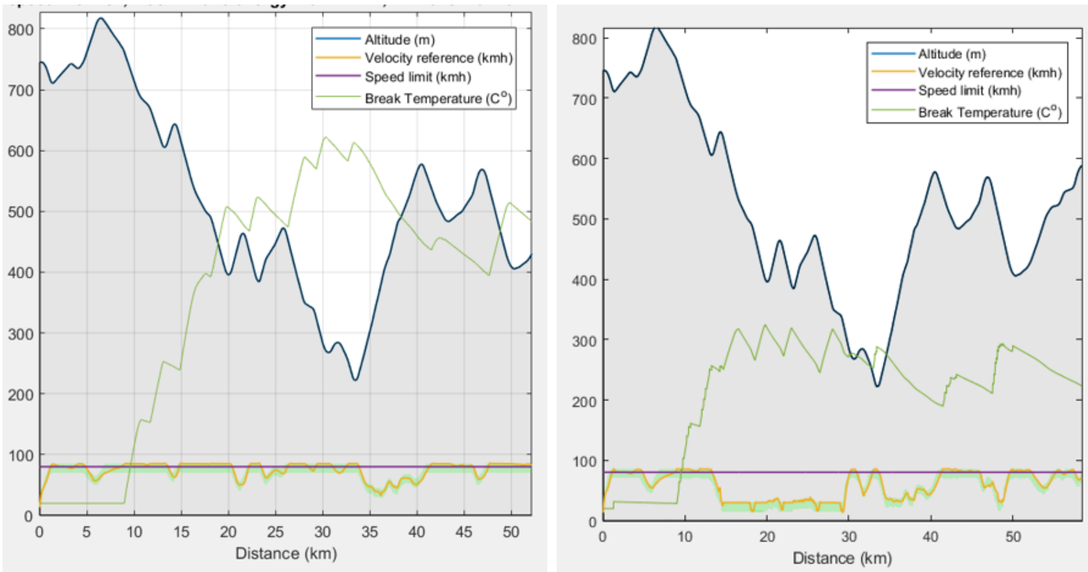

(a) Performance of the PEM controller for a section of cycle 3 and a 64 ton vehicle.

(b) Performance of Heur-PEM controller for a section of cycle 3 and a 64 ton vehicle.

Figure 5.5: Comparison between the original predictive controller and the Heur-PEM controller using an altered pre-filter algorithm.

Further, Figure 5.6 visualizes a comparison between different derate strategies in terms of the EM temperature profile. Just as before, the Heur-PEM performance is compared with a heuristic strategy without predictive information ("Heur") and the case when the EM is not derated ("None"). This is done for a section of cycle 3 and a 64 ton vehicle.

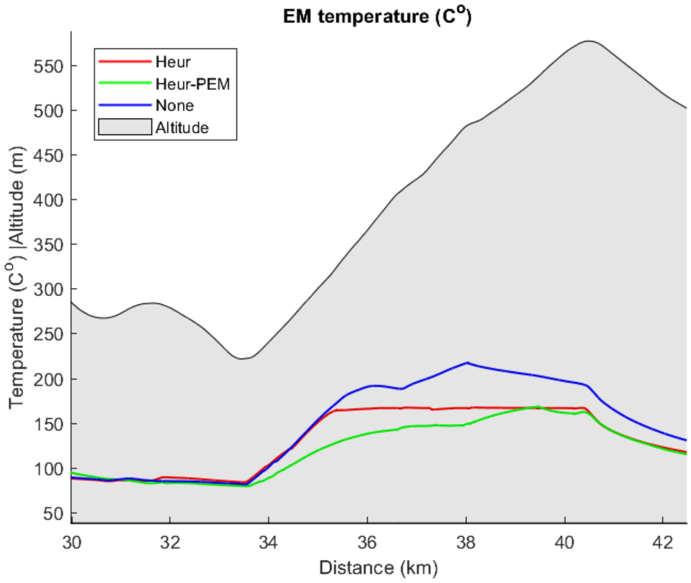

Figure 5.6: Comparison between three different derate strategies evaluated based on temperature. The studied case is cycle 3 with a 64 ton vehicle.

Comparing the EM power constraint between the 3 strategies yields the result displayed in Figure 5.7. Similarly, this is done for a section of cycle 3 and a 64 ton vehicle, just as above.

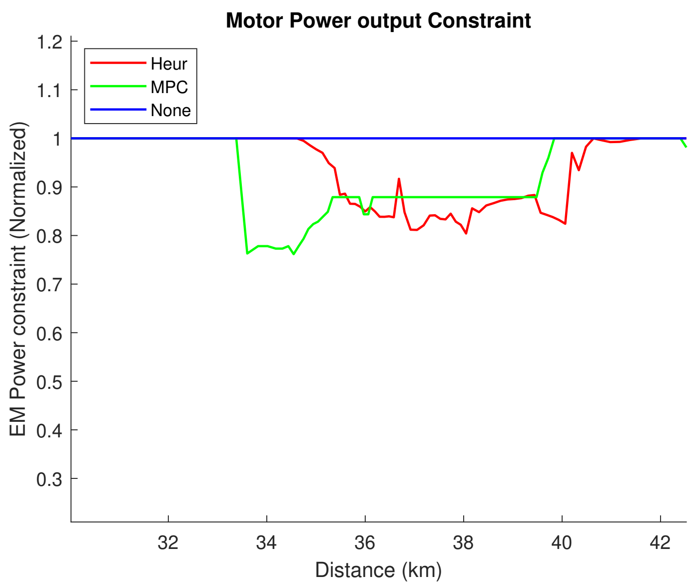

Figure 5.7: Comparison between three different EM derate strategies based on the power constraints on EM1. The studied case is a section of cycle 3 with a 64 ton vehicle.

In this case it is also of high interest to compare the computation time of the different solutions. Table 5.1 the computation for a single iteration of all investigated controllers. The time metric has been normalized based on the mean computation time of the current pre-filter algorithm. This is to mitigate the influence of factors such as hardware differences and to better show the relative time scales.

Table 5.1: Approximation of the average computation time for a single execution of the respective algorithm. All metrics are normalized based on the mean computation time of the current pre-filter algorithm

Controller	Mean Computation time (normalized)	Max Computation time (normalized)
Pre-filter	1	10
DP	$\sim$ 86	$\sim$ 205
Safe PEM	$\sim$ 500	$\sim$ 3 000
Safe PEM with EM derate	$\sim$ 8 000	$\sim$ 70 000
Altered Heuristic pre-filter	$\sim$ 30	$\sim$ 500

5.4 Summary

With all controllers introduced in a more qualitative fashion it becomes appropriate to make a more quantitative comparison between them. Tables 5.2, 5.3 and 5.4. compare the brake temperatures results of all 9 investigated controllers for cycles 1-3 using a 64 ton vehicle.

Table 5.2: Summary of the brake temperature results for all investigated controllers. The studied case is cycle 1 and a 64 ton vehicle

Controller	Description	Mean Speed (km/h)	Mean T_{brake} (°C)	Max T_{brake} (°C)
Static	Without predictive controller	79.7	72.0	165
PEM	Original predictive controller	79.2	35.2	86
Safe-PEM	Aggressive tuning	79.2	31.1	69
	Moderate tuning	79.2	31.1	68
	Conservative tuning	79.2	31.1	68
Safe-PEM with predictive derate	Aggressive tuning	79.1	31.3	69
	Moderate tuning	79.1	31.3	69
	Conservative tuning	79.1	31.2	69
Heur-PEM	Altered pre-filter algorithm	79.1	37.5	86

Table 5.3: Summary of the brake temperature results for all investigated controllers. The studied case is cycle 2 and a 64 ton vehicle

Controller	Description	Mean Speed (km/h)	Mean T_{brake} ($°C$)	Max T_{brake} ($°C$)
Static	Without predictive controller	77.7	132	472
PEM	Original predictive controller	76.8	77.4	361
Safe-PEM	Aggressive tuning	76.5	68.0	315.9
	Moderate tuning	76.4	68.2	317.8
	Conservative tuning	76.4	68.0	316.0
Safe-PEM with predictive derate	Aggressive tuning	76.3	69.5	316.5
	Moderate tuning	76.3	69.0	317.6
	Conservative tuning	76.3	68.5	313.6
Heur-PEM	Altered pre-filter algorithm	73.4	69.7	338.9

Table 5.4: Summary of the brake temperature results for all investigated controllers. The studied case is cycle 3 and a 64 ton vehicle

Controller	Description	Mean Speed (km/h)	Mean T_{brake} ($°C$)	Max T_{brake} ($°C$)
Static	Without predictive controller	70.9	311	689
PEM	Original predictive controller	69.5	261	622
Safe-PEM	Aggressive tuning	66.8	235	532
	Moderate tuning	63.9	188	408
	Conservative tuning	62.3	158	332
Safe-PEM with predictive derate	Aggressive tuning	66.0	235	534
	Moderate tuning	63.6	188	375
	Conservative tuning	61.4	158	336
Heur-PEM	Altered pre-filter algorithm	59.6	186	341

Further, table 5.5 compares the energy efficiency of the 9 investigated controllers for cycle 3 using a 64 ton vehicle.

Table 5.5: Energy consumption results for cycle 3 and a vehicle weight of 64 tons.

Controller	Description	Energy consumption per km (normalized)	Mean Speed (km/h)
PEM	Original predictive controller	1	69.5
Safe-PEM	Aggressive tuning	0.96	66.8
	Moderate tuning	0.90	63.9
	Conservative tuning	0.86	62.3
Safe-PEM with predictive derate	Aggressive tuning	0.96	65.9
	Moderate tuning	0.90	63.7
	Conservative tuning	0.87	61.4
Heur-PEM	Altered pre-filter algorithm	0.92	59.6

The EM temperature results for all 9 investigated controllers are displayed in table 5.6. The table cover cycle 3 using a 64 ton vehicle.

Table 5.6: EM temperature results for cycle 3 and a 64 ton vehicle.

Controller	Description	Mean Speed (km/h)	Time spent above 165 $°C$ (EM1 | EM2) (% of total cycle time)	Max T_{EMi} (EM1 | EM2) ($°C$)
Static with heuristic derate	Without predictive controller	70.9	20.32 | 20.20	168 | 168
PEM with heuristic derate	Original predictive controller	69.4	14.69 | 12.50	168 | 168
Safe-PEM	Aggressive tuning	62.3	11.01 | 8.54	168 | 168
	Moderate tuning	63.9	12.29 | 8.92	167.7 | 167.5
	Conservative tuning	66.8	13.92 | 10.09	167.7 | 167.5
Safe-PEM with predictive derate	Aggressive tuning	66.0	7.54 | 1.00	173 | 168
	Moderate tuning	63.6	7.61 | 0.47	178 | 168
	Conservative tuning	61.4	4.68 | 0.85	169 | 168
Heur-PEM	Altered pre-filter algorithm	59.6	0.78 | 0.22	168.8 | 165.5

Finally, tables 5.7, 5.8 and 5.9 displays the corresponding results for a 46 ton vehicle, this time only for cycle 3. The tables display the brake temperature, energy consumption and EM temperature results respectively.

Table 5.7: Summary of the brake temperature results for all investigated controllers. The studied case is cycle 3 and a 46 ton vehicle

Controller	Description	Mean Speed (km/h)	Mean T_{brake} ($°C$)	Max T_{brake} ($°C$)
Static	Without predictive controller	76.7	197.7	516.8
PEM	Original predictive controller	76.9	168.3	462.7
Safe-PEM	Aggressive tuning	76.1	157.8	422.7
	Moderate tuning	75.4	150.9	377.8
	Conservative tuning	74.3	138.9	315.2
Safe-PEM with predictive derate	Aggressive tuning	75.9	157.4	422.9
	Moderate tuning	75.3	151.6	377.6
	Conservative tuning	74.1	140.5	316.3
Heur-PEM	Altered pre-filter algorithm	70.1	148.1	310.4

Table 5.8: Energy consumption results for cycle 3 and a vehicle weight of 46 tons.

Controller	Description	Energy consumption per km (normalized)	Mean Speed (km/h)
PEM	Original predictive controller	1	76.9
Safe-PEM	Aggressive tuning	0.98	76.1
	Moderate tuning	0.97	74.5
	Conservative tuning	0.96	74.3
Safe-PEM with predictive derate	Aggressive tuning	0.98	75.9
	Moderate tuning	0.97	75.3
	Conservative tuning	0.96	75.9
Heur-PEM	Altered pre-filter algorithm	0.98	72.3

Table 5.9: EM temperature results for cycle 3 and a 46 ton vehicle.

Controller	Description	Mean Speed (km/h)	Time spent above 165 $°C$ (EM1 | EM2) (% of total cycle time)	Max T_{EMi} (EM1 | EM2) ($°C$)
Static with heuristic derate	Without predictive controller	76.7	7.78 | 7.87	167.5 | 167.6
PEM with heuristic derate	Original predictive controller	76.9	7.74 | 8.04	167.4 | 167.5
Safe-PEM	Aggressive tuning	76.1	7.40 | 8.36	167.3 | 167.5
	Moderate tuning	75.4	7.66 | 8.37	167.3| 167.4
	Conservative tuning	74.3	7.61 | 8.30	167.3 | 167.5
Safe-PEM with predictive derate	Aggressive tuning	75.9	6.71 | 5.45	175.9| 168.8
	Moderate tuning	75.3	6.75| 5.36	176.5 | 169.0
	Conservative tuning	74.1	6.94 | 6.36	175.9 | 168.8
Heur-PEM	Altered pre-filter algorithm	72.3	2.34 | 1.41	167.5 | 164.8

6

Discussion

6.1 Safe Braking

The scenario displayed in Figure 5.1 is the most challenging stretch for the brake system out of all of the investigated cycles. Since the overall purpose of this thesis is to achieve a safe and hence robust controller, this could also be considered as one of the most interesting examples. This is a clear case where the speed profile that is suggested by both the current PEM and the Static controllers causes dangerously high brake temperatures, well above $550C^o$. However, comparing figures 5.1a and 5.1b it becomes clear that it is possible to significantly reduce the brake temperature by limiting the speed using an optimal control approach. Not only is it possible to maintain the brake temperature below $550°C$, it also is possible to maintain the temperature well below $350°C$, almost a halve of the original. Again however, this does not come without certain drawbacks. The Safe-PEM speed profile can be seen to drop significantly, e.g. at $\sim 15km$, which results in an overall longer trip time. This is naturally undesirable, e.g.since costumers aim to minimize their delivery time.

A simple way to increase the speed of the vehicle is to allow the temperature to rise above $350°C$. The defined "critical limit" at $550°C$ should however be maintained. As can be seen in Figure 5.2 decreasing the cost on brake temperatures below $550C°$ causes both the brake temperature and speed to increase in correspondence. In practice this means that a costumer could tune the different costs at $300°C$ and $350°C$ to achieve a desirable trade-off.

The same behaviour that is visualized in figures 5.1 5.2 is also shown in a more quantitative fashion in table 5.4. All Safe-PEM controllers can decrease the temperature below the critical temperature limit at $550°C$ and the conservative tuning is further able to decrease the temperature below the danger limit at $350°C$. This also comes with a corresponding decrease in the average speed which naturally increase the total trip time. However, as also is introduced in table 5.5 the decrease in speed also corresponds to a more energy efficient solution. In the most conservative controller this corresponds to a significant decrease of 14% compared to the current PEM, which notably already is a significant improvement to the Static controller. The reason for this is most likely due to the fact that the mechanical brakes "consume" kinetic energy from the vehicle. By decreasing the vehicle speed appropriately, the power necessary to brake the vehicle is decreased accordingly. This means that the regenerative brake system can be responsible for a significantly larger portion of the power demand. Hence, kinetic energy that would otherwise be lost as heat in the mechanical brake discs, can instead be recuperated back into the power train and eventually be stored as chemical energy in the battery. I.e, the obtained controller is going to be slower, but it is simultaneously also going to be more energy efficient. This can instead be very attractive for a potential customer that wishes to increase the vehicle range for longer cycles, such as cycle 2 and cycle 3. This behaviour can again be tuned by utilising the three different cost parameters, as also illustrated in table 5.5.

In a broader scope, tables 5.2 and 5.3 that show the brake temperature results for cycle 1 and cycle 2, illustrates why it is possible to sometime ignore the brake temperature issue in practice. Since these cycles contain smaller changes in elevation, 122m difference for cycle 1 and 425m for cycle 2 as introduced in table 4.2, the demand on the brake system is not going to be as significant as to pose very dangerous scenarios in practice. Cycle 2 does however show some potential for dangerous scenarios which, as shown in table 5.3, is possible to avoid. Notably, when there is no need to alter the speed profile to account for a high brake temperature, the Safe PEM returns the same solutions as the previous PEM (with some marginal differences). These marginal differences could in turn simply be a result of the fact that the heuristic pre-filter naturally uses different conditions compared to the case of using optimal control, leading to some differences in the suggested velocity bound.

Finally, as illustrated in tables 5.7, 5.8 and 5.9 the weight of the vehicle plays a significant role in the brake power demand. Comparing between using a 46 and a 64 ton vehicle for cycle 3 it is e.g., shown that the maximum brake temperature deceases by 173°C. Other metrics also change accordingly e.g., the percentage of time spent at high EM temperatures which is consistently decreased for all controllers. In practical cases, reducing the vehicle weight even further and instead opting for a medium-duty truck, is typically also the only option that a customer can take to ensure a safe operation of the vehicle. This results in a lower amount of transported cargo per vehicle which becomes less efficient in terms of both energy usage and financial cost. However, as illustrated in this thesis, by using a predictive controller to ensure that the brake temperature is maintained below critical levels it is possible to ensure a safe operation in this regard and allow for the use of heavy-duty vehicles even in challenging terrain.

6.2 Safe Braking and Propulsion

The scenario displayed in Figure 5.3 shows a very challenging stretch for the EMs. As seen from the case when no EM power derate is performed, the temperature reaches well above 200°C which is significantly above the "critical" limit of 180°C. Comparing with the result obtained by the Safe-PEM controller it is clearly possible to constrain the motor power such that the temperature does not exceed 180°C in this case. However, it is also clear that the heuristic law can accomplish this task. By design this leads to a temperature profile that initially peaks at $\sim$ 167°C and remains at this level for the remaining duration of the uphill. Operating the EM at such a high temperature for a long period of time could potentially be harmful in terms of component health which could lead to failures in the long term. Investigating the EM temperature profile that is obtained by the Safe-PEM controller it can be observed that the temperature instead avoids this behaviour leading to an overall lower EM temperature. To exactly quantify this impact, it would however be necessary to perform a full SOH analysis. Sadly, this was not feasible in the scope of this thesis meaning that only qualitative conclusions can be drawn in this regard. What can be said is that the Safe-PEM controller successfully minimizes the amount of time that the EMs spend at very "high temperatures" defined by the constraint at $170°C$. At the same time the controller attempts to maximize the velocity based on the trade-off defined by the costs assigned in the objective function.

The same scenario is investigated in Figure 5.3 but here in terms of the EM power constraint. The existing heuristic controller does at first not constrain the EM for the initial $500m$ of the uphill ($\sim 34.5 - 36.5km$) and then gradually decreases the available power to $\sim 85\%$. This demonstrates the undesirable power drop causing a sharp decrease in the perceived drive-ability which further could lead to potentially dangerous driving scenarios. As previously stated, the ideal case in terms of drive-ability would be a direct constrain at the start of the hill $\sim 33.5km$ that eventually gets relaxed as the EMs are predicted to be able to remain below the critical limit. However, as is clear from the plot, this was not achievable using the Safe-PEM controller. Instead, what is observed are more rapid changes in the EM constraint which if anything, heightens the potential issues just raised. In this case, introducing a constraint on how fast the EM power is allowed to change as explained in Equation (3.13) did not resolve this issue. Many constraints off a similar fashion were also tested e.g., constraining changes in the temperature slack variables, but these approaches also gave the same rapid fluctuation in the EM power constraint. I would hypothesize that this behaviour is a direct result of the "Speed-EM temperature" trade-off. Seemingly, the highest speed possible that minimizes the cost in both these regards is obtained by performing short and sizeable decreases in power. This behaviour is also illustrated in other research such as *Wallscheid*, (*2017*) [46]. Additionally worth noting is that the Safe-PEM controller in this case attempts to constrain both the brake and the EM temperatures simultaneously. Solving the issue of obtaining the desired derate using MPC would likely require designing a controller with this specific intent which I think would require an intelligent design of constraints and of course more research. However, obtaining the desired behaviour using a sub-optimal heuristic controller using predictive models seems to be a simpler and much more feasible problem, as introduced in the following section.

A more quantitative analysis can be made based on table 5.6. Extending the Safe-PEM controller to also constrain the EM seems to have no negative effects concerning the problem of maintaining a safe brake temperature. In all three settings, Aggressive, Moderate and Conservative, the controller obtains almost identical brake temperature metrics which hence maintains the safety benefits introduced in the previous section. It is also clearer that the Safe-PEM controller significantly reduces the duration that the EMs are operated at high temperatures. In comparison with the PEM controller it is possible to lower the high EM1 temperatures by $\sim 300\%$

and the high EM2 temperatures are almost mitigated completely. This seems to qualitatively indicate that this control strategy would result in a significant improvement in terms of SOH, which would avoid the likelihood of system failures. Worth noting as well is that the recorded maximum EM temperatures are increased using the predictive derate Safe-PEM controller, which together with the other results seems to indicate that the EMs experience short spikes in temperatures. All of them are however maintained below the critical limit of $180°C$. One potential reason for this behaviour could again be motivated by the speed-EM temperature trade-off that seem to favour rapid changes in the power constraint. Again, to analyse this further a quantitative SOH analysis would likely be of high interest. What also is observed is a somewhat lower speed compared to the Safe-PEM controller which is using the current heuristic derate function. This is likely due to some inaccuracies in the model. What could be observed is that the predicted temperature on occasions would overestimate the EM motor temperature. This then leads to the engine being derated when not necessary, causing a lower vehicle speed. This could notably be a consequence of the harsh assumption that the temperature change is a first-order model with respect to temperature. To improve the model predictions and hence obtain a faster solution I would suggest studying higher-order models with more accurate temperature dependant heat transfer coefficients.

6.3 Heuristic Algorithm

Figure 5.5 displays the same challenging scenario that was discussed in the prior sections concerning the brake temperature. The Figure clearly shows that using this Heur-PEM controller it is possible to accomplish a strategy that ensures that the brake temperature is maintained below $550°C$ in this scenario, using the altered pre-filter algorithm. It is also possible to further reduce the temperature even below $350°C$ and obtain the same characteristic of the solution that was obtained for the Conservative Safe-PEM controller. Again, this is a significant improvement compared to the original PEM controller where the temperature peaks well above $550C\circ$. However, in this case the Heur-PEM controller suffers from a more significant decrease in speed. As observed in the Figure the speed drops significantly at $\sim 15km$ and maintains this velocity until the temperature is predicted to decrease sufficiently at $\sim 27km$. Comparing with the corresponding speed profile of the Safe-Pem controller displayed in Figure 5.1 this is a significant decrease. This is naturally since the Safe-PEM controller attempts to maximize the vehicle speed with an optimal control approach, which the Heur-PEM controller does not.

Further, Figure 5.6 displays the same challenging scenario that was discussed in the prior section concerning the EM temperature. In this case the Heur-PEM controller also shows a promising temperature profile. Instead of quickly increasing towards the critical limit, the temperature slowly increases in a smooth fashion and eventually peaks at $\sim 167°C$. This approach significantly decreases the amount of time that the engine operates at high temperatures, potentially also leading to a significant improvement in terms of SOH. It is also clear from Figure 5.4 that the EM is able to appropriately derate the engine prior to the uphill and avoid the drop in power that is obtained from the current heuristic approach used by the PEM and Safe-PEM controllers. By instead constraining the EM power at the start of the uphill, as is the case for the Heur-PEM controller, the driver does not experience this sudden drop which improves the perceived drive-ability. Further, as the truck traverses up the hill the EM power constraint is gradually relaxed to ensure that the EM temperature peaks close to the crest of the hill, contrary to both the PEM and the Safe-PEM controllers. Although this controller obtains the desired EM temperature and derate properties, it is sub-optimal in terms of maximizing the speed of the vehicle. Naturally, since the EM power is excessively decreased relative to the solution that maximizes the speed, the resulting speed profile will be slower overall in comparison with the other two alternatives.

The same behaviour that is illustrated in figures 5.5, 5.6 and 5.7 is also distinguishable in the quantitative analysis. Table 5.4 displays that the brake temperature can be limited below $350°C$ and table 5.6 shows that the EM temperatures can be limited below $180°C$. The duration of which the EM temperatures are high is also significantly reduced, almost to zero in comparison with the PEM controller. Note that the EM temperatures also peaks at lower temperatures compared to the Safe-PEM that include the EM temperatures. However, the significant drawback of this approach is that recommend speed profile on occasions is far from the optimal. By comparing the different "Energy Efficiency-Speed" trade-offs displayed in table 5.5 it becomes clear that the Heur-PEM controller is subpar all other controllers. As for the optimal controllers, a speed decreases corresponds to an increase in the recuperated energy, leading to an increased energy efficiency. The Heur-PEM controller, however, obtains the slowest policy without being the most energy efficient.

Finally, the perhaps most interesting metrics for the Heur-PEM controller are displayed in Figure 5.1. As the optimal solvers take an extensive amount of time to compute they are likely not feasible in a practical application. Some measures can of course be taken to significantly reduce this computation time, however it would likely be difficult to match the speed of the current pre-filter that simply computes a single forward-pass over the horizon. This is clear from the fact that all the introduced controllers have computation times several magnitudes larger than the mean of the current pre-filter. However, as can be seen by utilizing the heuristic algorithm it is possible to solve the brake and EM temperature problems while simultaneously maintaining a feasible computation time. Although it is several times slower than the current pre-filter, the computation is on the same magnitude as the current DP solver, potentially implying that the Heur-PEM controller could be feasible in a practical application.

7
Conclusions

A summary of the results and the points raised in the discussion is displayed in table 7.1. The "check marks" (✓) indicate that the respective controller could solve the specified problem and the "crosses" (×) indicate otherwise.

Table 7.1: A comparison between the different controllers in terms of accomplished tasks.

	Optimality	Brake temperature	EM temperature	Smooth EM derate	Practical feasibility
Current PEM	✓	×	×	×	✓
Safe-PEM	✓	✓	×	×	×
Safe-PEM with EM	✓	✓	✓	×	×
Heur-PEM	×	✓	✓	✓	✓

Finally, the presented results can be related to the main research questions.

- It was possible to ensure that the brake temperatures were maintained below the specified safety critical levels.
- It was possible to ensure that the EM temperatures were maintained below the specified safety critical levels.
- Using the constraints investigated it was not possible to obtain a "smooth" derate strategy using optimal control, while also maintaining the brake and EM temperatures below certain levels and optimizing for energy efficiency. It was however achievable using a heuristic algorithm.
- It was possible to approximate the optimal controllers and maintain the brake and EM temperatures at safe levels, while also obtaining a smooth derate. This yields a more practically feasible controller with sub-optimal performance in terms of energy efficiency.

In terms of future work, as illustrated by the heuristic approach, there is a good possibility of accomplishing a desirable motor derate strategy using the optimal control approach. One approach could be to separate the brake and EM problems to focus entirely on avoiding the behavior obtained via the "Speed-EM temperature" cost trade-off. Similarly, improving the EM temperature models using a higher-order model with more accurate, perhaps temperature dependant heat transfer coefficients. It could also be very interesting to analyse the results of this thesis using a quantitative SOH metric to clearly describe the potential improvements made by the predictive EM temperature controller.

On another note, it would also be very interesting to investigate if it is possible to utilize a prediction of the battery peak-power-ability. Since maximum energy that can be recuperated is mainly limited by the rate at which the battery can charge, utilizing the peak-power would further decrease the ability to limit the brake temperature and further improve the energy efficiency.

A very interesting improvement of the pre-filter algorithm would be to attempt to learn the generated decision log, using e.g., a reinforcement learning approach. Since the decisions taken by the algorithm simply amounts to using the maximum EM or brake power to speed up or down, there is in theory only two separate possible decision to take. The state of such an approach could then perhaps be defined based on the current velocity, brake temperature, EM temperatures and the upcoming inclination, which potentially could be expressive enough such that the reinforcement algorithm could learn to replicate the decisions of the Heur-PEM controller. The computational complexity would then reduce to a simple forward pass over the horizon, as is the case with the current pre-filter.

Bibliography

[1] *Setting CO2 emission performance standards for new heavy-duty vehicles and amending Regulations*. European Union. 2019.

[2] European Environment Agency. *Greenhouse gas emissions from transport in Europe*. URL: `https://www.eea.europa.eu/ims/greenhouse-gas-emissions-from-transport` (visited on 05/20/2022).

[3] Ahad Hamednia et al. "Computationally Efficient Algorithm for Eco-Driving Over Long Look-Ahead Horizons". In: *IEEE transactions on intelligent transportation systems* (2021).

[4] Ahad Hamednia et al. "Computationally Efficient Algorithm for Eco-Driving Over Long Look-Ahead Horizons". In: *IEEE transactions on intelligent transportation systems* (2021).

[5] G. P. Padilla, S. Weiland, and M. C. F. Donkers. "A Global Optimal Solution to the Eco-Driving Problem". In: *IEEE control system letters* (2018).

[6] Md. Abdus Samad Kamal et al. "Model Predictive Control of Vehicles on Urban Roads for Improved Fuel Economy". In: *IEEE transactions on control systems technology* (2013).

[7] Asim Rashid. "Overview of Disc Brakes and Related Phenomena - a review". In: *International Journal of Vehicle Noise and Vibration* (2014).

[8] Lino Guzzella and Antonio Sciarretta. "Vehicle Propulsion Systems: Introduction to Modeling and Optimization". In: Springer, 2005. Chap. 2, pp. 13–21.

[9] Rajesh Rajamani. "Vehicle Dynamics and Control". In: Springer, 2005. Chap. 4.1, pp. 95–110.

[10] James R. Welty, Gregory L. Rorrer, and David G. Foster. "Fundementals of Momentum, Heat and Mass Transfer". In: 6th ed. John Whiley & Sons, 2015. Chap. 12, p. 148.

[11] William Cai et al. "Review and Development of Electric Motor Systems and Electric Powertrains for New Energy Vehicles". In: *Automotive Innovation* (2021).

[12] Stephen J. Chapman. "Electric Machinery Fundamentals". In: 4th ed. The McGraw-Hill Companies, Inc, 2004. Chap. 4, pp. 230–267.

[13] Zeina Bitar and Samhi Al Jabih. "Studying the Performances of Induction Motor Used in Electric Car". In: *Energy Procedia* (2014).

[14] Anton Haumer and Christian Kral. "Motor Management of Permanent Magnet Synchronous Machines". In: *Proceedings of the 9th International Modelica Conference* (2012).

[15] Lino Guzzella and Antonio Sciarretta. “Vehicle Propulsion Systems: Introduction to Modeling and Optimization”. In: Springer, 2005. Chap. 4.5, pp. 89–105.

[16] *Bendix® ADB22X™, ADB22X-V™ Air Disc Brakes*. Bendix. 2013.

[17] Parth Girdhar et al. “Design and analysis of brake discs to improve performance in fade condition”. In: *AIP Conference Proceedings*. Vol. 2317. 1. AIP Publishing LLC. 2021, p. 040005.

[18] Jonathan Miller. “Advanced Braking Systems for Heavy Vehicles”. PhD thesis. University of Cambridge, 2010.

[19] William Leasure. *A factbook for the mechanical properties of the component for single-unit and articulated heavy trucks*. Tech. rep. The University of Michigan, Transportation Research Institute, 1986.

[20] Michiel Koot et al. “Energy management strategies for vehicular electric power systems”. In: *IEEE transactions on vehicular technology* 54.3 (2005), pp. 771–782.

[21] Zachary P. Cano et al. “Batteries and fuel cells for emerging electric vehicle markets”. In: *Nature Energy* (2018).

[22] John B. Goodenough and Kyu-Sung Park. “The Li-Ion Rechargeable Battery: A Perspective”. In: *Journal of The American Chemical Society* (2013).

[23] Peter Atkins, Loretta JOnas, and Leroy Laverman. “Chemical Principles: The Quest for Insight”. In: 7th ed. W.H. Freeman, 2016. Chap. 4.5, pp. 545–570.

[24] Bo Jiang et al. “Online Reliable Peak Charge/Discharge Power Estimation of Series-Connected Lithium-Ion Battery Packs”. In: *MPDI Energies* (2017).

[25] Ahad Hamednia et al. “Optimal Thermal Management, Charging, and Eco-driving of Battery Electric Vehicles”. In: *arXiv preprint arXiv:2205.01560* (2022).

[26] Rui Xiong et al. “Online estimation of peak power capability of Li-ion batteries in electric vehicles by a hardware-in-loop approach”. In: *Energies* 5.5 (2012), pp. 1455–1469.

[27] Lars Grune and Jurgen Pannek. “Non Linear Model Predictive Control”. In: Springer, 2011. Chap. 4, pp. 67–86.

[28] Lars Grune and Jurgen Pannek. “Non Linear Model Predictive Control”. In: Springer, 2011. Chap. 3, pp. 43–66.

[29] Stephan Wolf. “An Introduction to Duality in Convex Optimization”. In: *Seminar FI & IITM SS 2011* (2011).

[30] William Karush. “Minima of functions of several variables with inequalities as side constraints”. Master thesis. Department of Mathematics, University of Chicago, 1939.

[31] Harold W Kuhn and Albert W Tucker. “Nonlinear programming”. In: *Berkeley Symposium on Mathematical Statistics and Probability* (1951).

[32] Jon W. Tolle. “Nonlinear Programming”. In: *Encyclopedia of Physical Science and Technology* (2003).

[33] Gerhard Venter. “Review of optimization techniques”. In: (2010).

[34] Anders Forsgren, Philip E Gill, and Margaret H Wright. “Interior methods for nonlinear optimization”. In: *SIAM review* 44.4 (2002), pp. 525–597.

[35] Bo Egardt et al. "MODEL PREDICTIVE CONTROL LECTURE NOTES". MA thesis. Chalmers University of Technology, 2021.

[36] Nan Xu et al. "An Overview of Eco-Driving Theory, Capability Evaluation, and Training Applications". In: *MDPI Sensors* (2021).

[37] M.A.S. Kamal et al. "Ecological Vehicle Control on Roads with Up-Down Slopes". In: *IEEE Transaction on Intelligent Transportation Systems* (2010).

[38] Wissam Dib, Lorenzo Serrao, and Antonio Sciarretta. "Optimal Control to Minimize Trip Time and Energy Consumption in Electric Vehicles". In: *Optimal Control to Minimize Trip Time and Energy Consumption in Electric Vehicles* (2011).

[39] Toheed Ghandriz et al. "Real-time predictive energy management of hybrid electric heavy vehicles by sequential programming". In: *IEEE Transactions on Vehicular Technology* 70.5 (2021), pp. 4113–4128.

[40] Erik Hellström, Jan Åslund, and Lars Nielsen. "Management of kinetic and electric energy in heavy trucks". In: *SAE International Journal of Engines* 3.1 (2010), pp. 1152–1163.

[41] Nikolce Murgovski, Bo Egardt, and Magnus Nilsson. "Cooperative energy management of automated vehicles". In: *Control Engineering Practice* 57 (2016), pp. 84–98.

[42] Joel A E Andersson et al. "CasADi – A software framework for nonlinear optimization and optimal control". In: *Mathematical Programming Computation* 11.1 (2019), pp. 1–36. DOI: `10.1007/s12532-018-0139-4`.

[43] Andreas Wachter and Lorenz T Biegler. "On the implementation of an interior-point filter line-search algorithm for large-scale nonlinear programming". In: *Mathematical programming* 106.1 (2006), pp. 25–57.

[44] Joel Andersson, Joris Gillis, and Moritz Diehl. *User Documentation for CasADi v3.4.4*. URL: `http://casadi.sourceforge.net/v3.4.4/users_guide/casadi-users_guide.pdf` (visited on 05/19/2018).

[45] James R. Welty, Gregory L. Rorrer, and David G. Foster. "Fundementals of Momentum, Heat and Mass Transfer". In: 6th ed. John Whiley & Sons, 2015. Chap. 4, pp. 229–278.

[46] Oliver Wallscheid and Joachim Böcker. "Derating of automotive drive systems using model predictive control". In: *2017 IEEE International Symposium on Predictive Control of Electrical Drives and Power Electronics (PRECEDE)*. IEEE. 2017, pp. 31–36.

A

Complete Optimization Formulations and Derivations

A.1 Brake problem formulation

Below follows the complete, rigorous formulation of the optimization problem with the objective of ensuring that the brake temperatures are maintained to the selected limit. Fundamental relations that follow from section 3.1 and 4 are not repeated to condense the formulation.

Minimize,

$$\sum_{k=0}^{N-1} q_{11}\delta_1(k)^2 + q_{22}\delta_2(k)^2 + q_{33}\delta_3(k)^2 + q_{44}\delta_4(k)^2 + q_{55}\delta_5(k)^2 + \sum_{k=0}^{N-2} r_0 F_{brake}^2(k) \tag{A.1}$$

Subject to equality constraints,

$$E_k(k+1) = F_{EM,whl}(k) + F_{brake}(k) - \frac{C_d A_p \rho E_k(k)}{m} - m_v g(c_r \cos(\alpha(k)) + \sin(\alpha(k))) \tag{A.2a}$$

$$T_{brake}(k+1) = \frac{m_{disc}^{-1}}{\xi_0 + 2\xi_1 T_{brake}(k)} \left(\frac{1}{n_{truck}} F_{truck}(k) - \frac{1}{v(k)} A_d h\big(T_{brake}(k)\big)(T_{brake}(k) - T_{amb}) \right) \tag{A.2b}$$

$$C_{p,brake}(k) = \xi_0 + \xi_1 T_{brake}(k) \tag{A.2c}$$

$$F_{truck}(k) = \frac{1}{n_{whl}^{tru}} \left(F_{brake}(k) \exp(\frac{F_{brake}(k)}{F_{crit}}) + F_{brake,split}(k)\big(1 - \exp(\frac{F_{brake}(k)}{F_{crit}})\big) \right) \tag{A.2d}$$

$$F_{brake,split}(k) = C_{brake}^{tru} n_{whl}^{tru} \left(\frac{F_{brake}(k) + C_{brake}^{tra} n_{whl}^{tra} (P_0^{tra} - P_0^{tru})}{C_{brake}^{tru} n_{whl}^{tru} + C_{brake}^{tra} n_{whl}^{tra}} \right) \tag{A.2e}$$

$$E_k(0) = E_k(t), \quad T_{brake}(0) = T_{brake}(t), \quad k = 1, \dots N-2 \tag{A.2f}$$

and inequality constraints,

$$\frac{P_{bat}^{min}(s_0)}{v(k)\eta_{El}} \leq F_{EM}(k) \leq \eta_{El}\frac{P_{bat}^{max}(s_0)}{v(k)} \tag{A.3a}$$

$$F_{EM}(k) \leq \eta_{EM}\frac{P_{EM}^{max}(s_0)}{v(k)} \tag{A.3b}$$

$$F_{EM}(k) \leq ma_{max} + \frac{C_d A_p \rho v(k)^2}{2} + c_r mg\cos(\alpha(k)) + mg\sin(\alpha(k)) \tag{A.3c}$$

$$F_{brake}(k) \geq -ma_{max} + \frac{P_{bat}^{min}(s_0)}{v(k)\eta_{El}} + \frac{C_d A_p \rho v(k)^2}{2} + c_r mg\cos(\alpha(k)) + mg\sin(\alpha(k)) \tag{A.3d}$$

$$F_{brake}(k) \leq 0 \tag{A.3e}$$

$$E_{ref}(k) - \delta_1(k) \leq E_k(k) \leq E_{ref}(k) + \delta_2(k) \tag{A.3f}$$

$$T_{brake}(k) \leq 300 + \delta_3(k) \tag{A.3g}$$

$$T_{brake}(k) \leq 350 + \delta_4(k) \tag{A.3h}$$

$$T_{brake}(k) \leq 550 + \delta_5(k) \tag{A.3i}$$

$$\delta_i(k) \geq 0, i = 1, 2, 3, 4, 5 \tag{A.3j}$$

(A.3k)

A.2 Brake problem and propulsion formulation

Below follows the complete, rigorous formulation of the optimization problem with the objective of ensuring that the brake and EM temperatures are maintain at their respective limits. Fundamental relations that follow from section 3.1, section 3.2 and 4 are not repeated to condense the formulation.

Minimize,

$$\begin{aligned}\sum_{k=0}^{N-1} q_{11}\delta_1(k)^2 &+ q_{22}\delta_2(k)^2 + q_{33}\delta_3(k)^2 + q_{44}\delta_4(k)^2 + q_{55}\delta_5(k)^2 + \\ + q_{66}\delta_6(k)^2 &+ q_{77}\delta_7(k)^2 + \sum_{k=0}^{N-2} r_0 F_{brake}^2(k)\end{aligned} \tag{A.4}$$

Subject to equality constraints,

$$E_k(k+1) = F_{EM,whl}(k) + F_{brake}(k) - \frac{C_d A_p \rho E_k(k)}{m} - m_v g(c_r\cos(\alpha(k)) + \sin(\alpha(k))) \tag{A.5a}$$

$$T_{brake}(k+1) = \frac{m_{disc}^{-1}}{\xi_0 + 2\xi_1 T_{brake}(k)}\left(\frac{1}{n_{truck}}F_{truck}(k) - \frac{1}{v(k)}A_d h\big(T_{brake}(k)\big)(T_{brake}(k) - T_{amb})\right) \tag{A.5b}$$

$$T_{EM1}(k) = \frac{1}{v(k)}\left(\beta_0(s_0)P_{EM,loss}(\omega_{EM1}(k), \mathcal{T}_{EM1}(k)) + \beta_1(s_0)(T_{EM1}(k) - T_{amb})\right) \tag{A.5c}$$

$$T_{EM2}(k) = \frac{1}{v(k)}\left(\beta_0(s_0)P_{EM,loss}(\omega_{EM2}(k), \mathcal{T}_{EM2}(k)) + \beta_1(s_0)(T_{EM2}(k) - T_{amb})\right) \tag{A.5d}$$

$$C_{p,brake}(k) = \xi_0 + \xi_1 T_{brake}(k) \tag{A.5e}$$

$$F_{truck}(k) = \frac{1}{n_{whl}^{tru}}\left(F_{brake}(k)\exp\Big(\frac{F_{brake}(k)}{F_{crit}}\Big) + F_{brake,split}(k)\big(1 - \exp\big(\frac{F_{brake}(k)}{F_{crit}}\big)\big)\right) \tag{A.5f}$$

$$F_{brake,split}(k) = C_{brake}^{tru} n_{whl}^{tru}\left(\frac{F_{brake}(k) + C_{brake}^{tra} n_{whl}^{tra}(P_0^{tra} - P_0^{tru})}{C_{brake}^{tru} n_{whl}^{tru} + C_{brake}^{tra} n_{whl}^{tra}}\right) \tag{A.5g}$$

$$P_{Heat,EM}(s) = \sigma_0\omega_{EMi}(s) + \sigma_1\omega_{EMi}^2(s) + \sigma_2\mathcal{T}_{EMi}^2(s) + \sigma_3\mathcal{T}_{EMi}^4(s) \tag{A.5h}$$

$$\omega_{EM1}(k) = \frac{R(\gamma_1(k, s_0))}{r_{whl}}v(k) \tag{A.5i}$$

$$\omega_{EM2}(k) = \frac{R(\gamma_2(k, s_0))}{r_{whl}}v(k) \tag{A.5j}$$

$$\mathcal{T}_{EM1}(k) = \frac{1}{R(\gamma_1(k, s_0))}F_{EM,whl}(k) \tag{A.5k}$$

$$\mathcal{T}_{EM2}(k) = \frac{1}{R(\gamma_2(k, s_0))}F_{EM,whl}(k), \quad k = 1, \dots N-2 \tag{A.5l}$$

$$E_k(0) = E_k(t), \quad T_{brake}(0) = T_{brake}(t), \quad T_{EM1}(0) = T_{EM,1}(t), \quad T_{EM2}(0) = T_{EM,2}(t) \tag{A.5m}$$

and inequality constraints,

$$\frac{P_{bat}^{min}(s_0)}{v(k)\eta_{El}} \leq F_{EM}(k) \leq \eta_{El}\frac{P_{bat}^{max}(s_0)}{v(k)} \tag{A.6a}$$
$$F_{EM}(k) \leq \eta_{EM}\frac{P_{EM}^{max}(s_0)}{v(k)} \tag{A.6b}$$
$$F_{EM}(k) \leq ma_{max} + \frac{C_d A_p \rho v(k)^2}{2} + c_r mg\cos(\alpha(k)) + mg\sin(\alpha(k)) \tag{A.6c}$$
$$F_{brake}(k) \geq -ma_{max} + \frac{P_{bat}^{min}(s_0)}{v(k)\eta_{El}} + \frac{C_d A_p \rho v(k)^2}{2} + c_r mg\cos(\alpha(k)) + mg\sin(\alpha(k)) \tag{A.6d}$$
$$F_{brake}(k) \leq 0 \tag{A.6e}$$
$$E_{ref}(k) - \delta_1(k) \leq E_k(k) \leq E_{ref}(k) + \delta_2(k) \tag{A.6f}$$
$$F_{EM}(k) - \Delta_{F_{EM}}(k) \leq F_{EM}(k+1) \leq F_{EM}(k) + \Delta_{F_{EM}}(k) \tag{A.6g}$$
$$T_{brake}(k) \leq 300 + \delta_3(k) \tag{A.6h}$$
$$T_{brake}(k) \leq 350 + \delta_4(k) \tag{A.6i}$$
$$T_{brake}(k) \leq 550 + \delta_5(k) \tag{A.6j}$$
$$T_{EM1}(k) \leq 170 + \delta_6(k) \tag{A.6k}$$
$$T_{EM2}(k) \leq 170 + \delta_7(k) \tag{A.6l}$$
$$\delta_i \geq 0, \quad i = 1,2,3,4,5,6,7 \tag{A.6m}$$

A.3 Kinetic Energy Variable Change Derivation

The following section outlines the derivation for introducing a change from the velocity state to a kinetic energy state. This procedure has been clearly described in existing literature. The force balance equations are introduced in section 2.1.2, repeated for convenience,

$$\begin{aligned}
m_v\frac{\partial^2}{\partial t^2}x(t) &= F_{EM,whl}(t) + F_{brake}(t) + F_{roll}(t) + F_{g,plane}(t) + F_{drag}(t) \\
F_{drag}(t) &= -Cv(t)^2 = -\frac{C_d A_p \rho v(t)^2}{2} \\
F_{roll}(t) &= -c_r F_N(t) = -c_r m_v g\cos(\alpha(t)) \\
F_{g,plane}(t) &= -m_v g\sin(\alpha(t))
\end{aligned} \tag{A.7}$$

Applying the chain rule to the left-hand side (LHS) of the force balance,

$$m_v\frac{\partial^2 x(t)}{\partial t^2} = m_v\frac{\partial v(t)}{\partial t} = m_v\frac{\partial v(s)}{\partial s}\frac{\partial s}{\partial t} = m_v\frac{\partial v(s)}{\partial s}v(s) \tag{A.8}$$

Similarly for the kinetic energy of the vehicle,

$$\begin{aligned}
E_k(t) &= \frac{m_v v(t)^2}{2} \\
\frac{\partial E_k(t)}{\partial t} &= \frac{\partial E_k(s)}{\partial s}\frac{\partial s}{\partial t} = \left(m_v\frac{\partial v(s)}{\partial s}v(s)\right)v(s) \\
\Rightarrow \frac{\partial E_k(s)}{\partial s} &= m_v\frac{\partial v(s)}{\partial s}v(s)
\end{aligned} \tag{A.9}$$

I.e, the (LHS) of the force balance can be replaced with the position derivative of the kinetic energy.

The inclination can now be described by a function of distance $\alpha(s)$. This simply yields the retarding forces as,

$$\begin{aligned} F_{drag}(s) &= -\frac{C_d A_p \rho v(s)^2}{2} = -\frac{C_d A_p \rho E_k(s)}{m} \\ F_{roll}(s) &= -c_r F_N(s) = -c_r m_v g \cos(\alpha(s)) \\ F_{g,plane}(s) &= -m_v g \sin(\alpha(s)) \end{aligned} \tag{A.10}$$

Similarly $F_{EM,whl}(t), F_{brake}(t)$ represent control signals that can be defined over s. By finally considering a discretized model the the expression becomes,

$$E_k(k+1) = F_{EM,whl}(k) + F_{brake}(k) - \frac{C_d A_p \rho E_k(k)}{m} - m_v g(c_r \cos(\alpha(k)) + \sin(\alpha(k))) \tag{A.11}$$

A.4 Brake Temperature Model Derivation

The following section outlines the derivation of the brake temperature model introduced in section 4.2. The section introduces the fundamental heat transfer relations, repeated for convenience. The relation is first derived in time and the converted to distance in a fashion similar to the previous section A.3.

$$\begin{aligned} \frac{\partial}{\partial t}\left(H_{internal}(t)\right) &= \frac{1}{n_{truck}}\left(H_{in}(t) - H_{out}(t)\right) \\ H_{internal}(t) &= m_{disc} C_{p,brake}(t) T_{brake}(t) \\ H_{in}(t) &= F_{truck}(t) v(t) \\ H_{out}(t) &= n_{truck} A_d h\Big(T_{brake}(t)\Big)(T_{brake}(t) - T_{amb}) \\ C_{p,brake}(t) &= \xi_0 + \xi_1 T_{brake}(t) \end{aligned} \tag{A.12}$$

First, since the specific heat capacity $C_{p,brake}(t)$ is temperature dependant the product rule needs to be applied on the right hand side of the heat balance. I.e,

$$\begin{aligned} \frac{\partial}{\partial t}\left(H_{internal}(t)\right) &= \frac{\partial}{\partial t}\left(m_{disc} C_{p,brake}(t) T_{brake}(t)\right) \\ &= m_{disc}\left(\frac{\partial C_{p,brake}(t)}{\partial t} T_{brake}(t) + \frac{\partial T_{brake}(t)}{\partial t} C_{p,brake}(t)\right) \\ &= m_{disc}\left(\xi_1 \frac{\partial T_{brake}(t)}{\partial t} T_{brake}(t) + \frac{\partial T_{brake}(t)}{\partial t}(\xi_0 + \xi_1 T_{brake}(t))\right) \\ &= m_{disc}\big(\xi_0 + 2\xi_1 T_{brake}(t)\big)\frac{\partial T_{brake}(t)}{\partial t} \end{aligned} \tag{A.13}$$

No significant derivations need to be made for the heat output $H_{out}(t)$ but this is not the case for the heat input $H_{in}(t)$. For cases when the trailer brake system is not engaged. We simply have that the total brake force is equal to the brake force on the truck, i.e

$$F_{brake}(t) = F_{truck}^{tot}(t) \tag{A.14}$$

However, when the trailer brake system is engaged this system is also added as,

$$F_{brake}(t) = F^{tot}_{truck}(t) + F^{tot}_{trailer}(t) \tag{A.15}$$

further Equation (2.9) yields,

$$F_{brake}(t) = C^{tru}_{brake} n^{tru}_{whl} (P_c(t) - P^{tru}_0) + C^{tra}_{brake} n^{tra}_{whl} (P_c(t) - P^{tra}_0) \tag{A.16}$$

which can be reformulated to express the total requested brake chamber pressure,

$$P_c(t) = \frac{F_{brake}(t) + C^{tru}_{brake} n^{tru}_{whl} P^{tru}_0 + C^{tra}_{brake} n^{tra}_{whl} P^{tra}_0}{C^{tru}_{brake} n^{tru}_{whl} + C^{tra}_{brake} n^{tra}_{whl}} \tag{A.17}$$

This means that the truck brake force when both brake systems are engaged, referred henceforth as $F_{truck,split}$, can be expressed as yields,

$$\begin{aligned} F_{brake,split}(t) =& C^{tru}_{brake} n^{tru}_{whl} \left(\frac{F_{brake}(t) + C^{tru}_{brake} n^{tru}_{whl} P^{tru}_0 + C^{tra}_{brake} n^{tra}_{whl} P^{tra}_0}{C^{tru}_{brake} n^{tru}_{whl} + C^{tra}_{brake} n^{tra}_{whl}} - P^{tru}_0 \right) \\ =& C^{tru}_{brake} n^{tru}_{whl} \left(\frac{F_{brake}(k) + C^{tra}_{brake} n^{tra}_{whl} (P^{tra}_0 - P^{tru}_0)}{C^{tru}_{brake} n^{tru}_{whl} + C^{tra}_{brake} n^{tra}_{whl}} \right) \end{aligned} \tag{A.18}$$

By defining a "critical transition force" F_{crit} based on a predefined total brake pressure $P_{c,crit}$ and Equation (A.15) to describe when the trailer brake system is engaged, it becomes possible to approximate the discontinuous function as,

$$F_{truck}(t) = \frac{1}{n^{tru}_{whl}} \left(F_{brake}(k) \exp(\frac{F_{brake}(k)}{F_{crit}}) + F_{brake,split}(k)\big(1 - \exp(\frac{F_{brake}(k)}{F_{crit}})\big) \right) \tag{A.19}$$

which was chosen by designed to be smooth and always overestimate the brake force of the physical system. With the above equation and Equations (A.12) and (A.13) it then becomes possible to derive the used physical temperature model. Discretizing and swapping the dependant variable from time to space yields,

$$T_{brake}(k+1) = \frac{m^{-1}_{disc}}{\xi_0 + 2\xi_1 T_{brake}(k)} \left(\frac{1}{n_{truck}} F_{truck}(k) - \frac{1}{v(k)} A_d h\big(T_{brake}(k)\big)(T_{brake}(k) - T_{amb}) \right) \tag{A.20}$$

A.5 EM Temperature Model Derivation

Similarly, the following section outlines the derivation of the EM temperature model introduced in section 4.3. The section introduces the fundamental heat transfer relations, repeated again for convenience. The relation is first derived in time and the converted to distance in a fashion similar to the previous section A.3. The index $i = 1, 2$ referrers to each respective engine, which are modeled identically.

$$\begin{aligned} &\frac{\partial}{\partial t}\left(H_{internal,i}(t)\right) = \left(H_{in,i}(t) - H_{out,i}(t)\right) \\ &H_{internal}(t) = m_{EMi} C_{p,EM} T_{EMi}(t) \\ &H_{in,i}(t) = P_{Heat,EM}(s) = \sigma_0 \omega_{EMi}(s) + \sigma_1 \omega^2_{EMi}(s) + \sigma_2 \mathcal{T}^2_{EMi}(s) + \sigma_3 \mathcal{T}^4_{EMi}(s) \\ &H_{out}(t) = A_{EM} h_{EM} (T_{EMi}(t) - T_{amb}) \\ &\omega_{EMi}(t) = \frac{R(\gamma_i)}{r_{whl}} v(t), \quad \mathcal{T}_{EMi}(t) = \frac{1}{R(\gamma_i)} F_{EM,whl}(t), i = 1, 2 \end{aligned} \tag{A.21}$$

Following the derivation of the variable change and discretization in section A.3 with the fact the heat transfer and specific heat coefficients are assumed to be constant with temperature, the derivation becomes straight forward. Simply inserting the above equations into the heat balance and re-arranging yields,

$$\frac{\partial T_{EMi}(t)}{\partial t} = \frac{1}{m_{EMi}C_{p,EM}} \left(P_{EM,loss}(\omega_{EMi}(t), \mathcal{T}_{EMi}(t)) + A_{EM}h_{EM}(T_{EMi}(t) - T_{amb})\right) \quad \text{(A.22)}$$

The adaptive coefficients $\boldsymbol{\beta}(t)$ are then introduced to describe temperature changes. These are initialized as,

$$\beta_0(0) = \frac{1}{m_{EMi}C_{p,EM}}, \quad \beta_1(0) = \frac{A_{EM}h_{EM}}{m_{EMi}C_{p,EM}} \quad \text{(A.23)}$$

and further update in real time using the extended kalman filter. This simplifies the temperature model as,

$$\frac{\partial T_{EMi}(t)}{\partial t} = (\beta_0(t)P_{EM,loss}(\omega_{EMi}(t), \mathcal{T}_{EMi}(t)) + \beta_1(t)(T_{EMi}(t) - T_{amb})) \quad \text{(A.24)}$$

Performing the variable change and discretizing in space then yields the final temperature model as,

$$T_{EM1}(k) = \frac{1}{v(k)} (\beta_0(s_0)P_{EM,loss}(\omega_{EM1}(k), \mathcal{T}_{EM1}(k)) + \beta_1(s_0)(T_{EM1}(k) - T_{amb})) \quad \text{(A.25)}$$

Note that the adaptive parameters are dependant on s_0 which corresponds to the position of the real time system at time t. The parameters are hence assumed constant for all k over the prediction horizon.

B

Supplementary Results

This section covers additional results for the wight-cycle combinations that where not mentioned further in the discussion and conclusion sections.

Table B.1: Summary of the brake temperature results for all investigated controllers. The studied case is cycle 1 and a 46 ton vehicle

Controller	Description	Mean Speed (km/h)	Mean T_{brake} ($C°$)	Max T_{brake} ($C°$)
Static	Without predictive controller	80.0	41.5	102.5
PEM	Original predictive controller	80.9	26.3	46.9
Safe-PEM	Aggressive tuning	80.8	24.2	40.4
	Moderate tuning	80.8	24.4	41.3
	Conservative tuning	80.8	24.4	41.3
Safe-PEM with predictive derate	Aggressive tuning	80.7	24.0	39.4
	Moderate tuning	80.7	24.0	39.4
	Conservative tuning	80.7	24.0	39.4
Heur-PEM	Altered pre-filter algorithm	80.8	26.1	46.4

Table B.2: Summary of the brake temperature results for all investigated controllers. The studied case is cycle 2 and a 46 ton vehicle

Controller	Description	Mean Speed (km/h)	Mean T_{brake} ($C°$)	Max T_{brake} ($C°$)
Static	Without predictive controller	79.6	100.1	377.1
PEM	Original predictive controller	79.8	59.7	261.4
Safe-PEM	Aggressive tuning	79.5	51.1	218.9
	Moderate tuning	79.5	50.7	216.7
	Conservative tuning	79.5	51.3	219.0
Safe-PEM with predictive derate	Aggressive tuning	79.5	51.3	217.9
	Moderate tuning	79.5	51.3	217.1
	Conservative tuning	79.5	51.3	219.3
Heur-PEM	Altered pre-filter algorithm	79.5	51.3	218.9

Table B.3: Energy consumption results for cycle 1 and a vehicle weight of 46 tons.

Controller	Description	Energy consumption per km (normalized)	Mean Speed (km/h)
PEM	Original predictive controller	1	80.9
Safe-PEM	Aggressive tuning	~ 1	80.8
	Moderate tuning	~ 1	80.8
	Conservative tuning	~ 1	80.8
Safe-PEM with predictive derate	Aggressive tuning	0.99	80.7
	Moderate tuning	0.99	80.7
	Conservative tuning	0.99	80.7
Heur-PEM	Altered pre-filter algorithm	~ 1	80.6

Table B.4: Energy consumption results for cycle 2 and a vehicle weight of 46 tons.

Controller	Description	Energy consumption per km (normalized)	Mean Speed (km/h)
PEM	Original predictive controller	1	79.8
Safe-PEM	Aggressive tuning	0.98	79.5
	Moderate tuning	0.98	79.5
	Conservative tuning	0.98	79.5
Safe-PEM with predictive derate	Aggressive tuning	0.98	79.5
	Moderate tuning	0.98	79.5
	Conservative tuning	0.98	79.5
Heur-PEM	Altered pre-filter algorithm	0.98	79.5

Table B.5: Energy consumption results for cycle 1 and a vehicle weight of 64 tons.

Controller	Description	Energy consumption per km (normalized)	Mean Speed (km/h)
PEM	Original predictive controller	1	79.2
Safe-PEM	Aggressive tuning	~ 1	79.2
	Moderate tuning	~ 1	79.2
	Conservative tuning	~ 1	79.2
Safe-PEM with predictive derate	Aggressive tuning	~ 1	79.1
	Moderate tuning	~ 1	79.1
	Conservative tuning	~ 1	79.1
Heur-PEM	Altered pre-filter algorithm	~ 1	79.1

Table B.6: Energy consumption results for cycle 2 and a vehicle weight of 64 tons.

Controller	Description	Energy consumption per km (normalized)	Mean Speed (km/h)
PEM	Original predictive controller	1	76.8
Safe-PEM	Aggressive tuning	0.98	76.5
	Moderate tuning	0.98	76.4
	Conservative tuning	0.98	76.4
Safe-PEM with predictive derate	Aggressive tuning	0.98	76.3
	Moderate tuning	0.98	76.3
	Conservative tuning	0.98	76.3
Heur-PEM	Altered pre-filter algorithm	0.98	73.4

Table B.7: Summary of the EM temperature results for all investigated controllers. The studied case is cycle 1 and a 46 ton vehicle

Controller	Description	Mean Speed (km/h)	Time spend above 165 $C°$ (EM1 | EM2) (% of total cycle time)	Max $T_{EM,i}$ (EM1 | EM2) ($C°$)
Static	Without predictive controller	80.0	0.00 | 0.00	132.1 | 137.5
PEM	Original predictive controller	80.9	0.00 | 0.00	133.9 | 115.9
Safe-PEM	Aggressive tuning	80.8	0.00 | 0.00	134.2 | 166.8
	Moderate tuning	80.8	0.00 | 0.00	134.4 |117.0
	Conservative tuning	80.8	0.00 | 0.00	134.4 |117.0
Safe-PEM with predictive derate	Aggressive tuning	80.7	0.00 | 0.00	134.0 |116.8
	Moderate tuning	80.7	0.00 | 0.00	134.0 |116.8
	Conservative tuning	80.7	0.00 | 0.00	134.0 |116.8
Heur-PEM	Altered pre-filter algorithm	80.8	0.00 | 0.00	140.1 |126.8

Table B.8: Summary of the EM temperature results for all investigated controllers. The studied case is cycle 2 and a 46 ton vehicle

Controller	Description	Mean Speed (km/h)	Time spend above 165 $C°$ (EM1 | EM2) (% of total cycle time)	Max $T_{EM,i}$ (EM1 | EM2) ($C°$)
Static	Without predictive controller	79.6	1.84 | 2.15	167.2 | 167.5
PEM	Original predictive controller	79.8	0.17 | 1.10	166.9 | 167.2
Safe-PEM	Aggressive tuning	79.5	0.00 | 1.10	164.5 | 167.3
	Moderate tuning	79.5	0.00 | 1.10	164.9 | 167.3
	Conservative tuning	79.5	0.00 | 1.07	164.9 | 167.3
Safe-PEM with predictive derate	Aggressive tuning	79.5	0.00 | 1.03	167.8 | 168.4
	Moderate tuning	79.5	0.00 | 1.03	167.8 | 168.3
	Conservative tuning	79.5	0.00 | 1.04	167.4 | 168.4
Heur-PEM	Altered pre-filter algorithm	79.5	0.53 | 1.10	170.4 | 168.9

Table B.9: EM temperature results for cycle 1 and a 64 ton vehicle.

Controller	Description	Mean Speed (km/h)	Time spent above 165 $°C$ (EM1 | EM2) (% of total cycle time)	Max T_{EMi} (EM1 | EM2) ($°C$)
Static with heuristic derate	Without predictive controller	79.7	0.00 | 0.00	156.7. | 160.6
PEM with heuristic derate	Original predictive controller	79.2	0.00 | 0.00	152.2 | 134.2
Safe-PEM	Aggressive tuning	79.2	0.00 | 0.00	153.4 | 135.8
	Moderate tuning	79.2	0.00 | 0.00	153.3 | 135.9
	Conservative tuning	79.2	0.00 | 0.00	153.3 | 135.8
Safe-PEM with predictive derate	Aggressive tuning	79.1	0.00 | 0.00	155.6 | 134.4
	Moderate tuning	79.1	0.00 | 0.00	155.6 | 134.4
	Conservative tuning	79.1	0.00 | 0.00	155.6 | 134.4
Heur-PEM	Altered pre-filter algorithm	79.1	0.00 | 0.00	147.6 | 133.3

Table B.10: EM temperature results for cycle 2 and a 64 ton vehicle.

Controller	Description	Mean Speed (km/h)	Time spent above 165 $°C$ (EM1 | EM2) (% of total cycle time)	Max T_{EMi} (EM1 | EM2) ($°C$)
Static with heuristic derate	Without predictive controller	77.7	4.57 | 4.32	167.5 | 167.5
PEM with heuristic derate	Original predictive controller	76.8	2.87 | 2.58	167.5 | 167.5
Safe-PEM	Aggressive tuning	76.5	2.46 | 1.99	167.5 | 167.5
	Moderate tuning	76.4	2.40 | 2.00	167.5 | 167.5
	Conservative tuning	76.4	2.38 | 1.99	167.5 | 167.5
Safe-PEM with predictive derate	Aggressive tuning	76.3	2.17 | 0.69	176.7 | 168.3
	Moderate tuning	76.3	2.60 | 0.84	177.0 | 168.3
	Conservative tuning	76.3	2.48 | 0.92	176.4 |168.4
Heur-PEM	Altered pre-filter algorithm	73.4	179.3 | 168.1	1.24 | 1.45

DEPARTMENT OF ELECTRICAL ENGINEERING
CHALMERS UNIVERSITY OF TECHNOLOGY
Gothenburg, Sweden
www.chalmers.se

CHALMERS
UNIVERSITY OF TECHNOLOGY